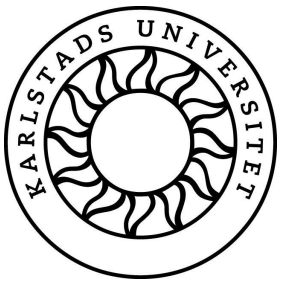

Additives in a steam engine to decrease friction

Friction testing of solid lubricants in powder form

Tillsatser i en ångmotor för att minska friktion

Friktionstester av fasta smörjmedel i pulverform

Viktor Lange

Faculty of Health, Science and Technology

Master of Science in Mechanical Engineering, Materials Engineering

Master thesis 30 HP

Supervisor: Pavel Krakhmalev

Co-supervisor: Mikael Fallqvist

Examiner: Mikael Grehk

2023-06-27

Abstract

This thesis aims to investigate the coefficient of friction between steel on steel contacts with the addition of solid lubricants such as h-BN, WS_2, MoS_2 in powder form, in dry conditions and wet conditions. More specifically, the purpose is to enhance the sliding between the piston rings and cylinder block in a modern high temperature steam engine developed by RANOTOR. The friction test was carried out as a linear sliding test with determined loads and sliding speed. Hertzian contact theory was deployed to calculate contact pressure and shear stresses to make sure the contact was elastic, alternatively plastic. It was found that WS_2 and MoS_2 lowered the coefficient of friction quite heavily in dry conditions, acting as a thin protective-lubricating film. h-BN performed rather poorly, increasing the coefficient of friction. In a water slurry, none of the powders managed to decrease the COF due to the particles not interacting with the surfaces.The solid lubricants tested should be further tested as coatings since they acted like it in dry conditions.

Sammanfattning

Denna rapport syftar till att undersöka friktionskoefficienten i stålkontakter med tillsats av fasta smörjmedel som h-BN, WS_2, MoS_2 i pulverform, under torra och våta förhållanden. Mer specifikt är syftet att förbättra glidningen mellan kolvringarna och insidan av cylindern i en modern högtemperatur-ångmotor utvecklad av RANOTOR. Friktionstestet genomfördes som ett linjärt glidtest med bestämda belastningar och glidhastighet. Hertzian-kontaktteorin användes för att beräkna kontakttryck och skjuvspänningar för att säkerställa att kontakten var elastisk alternativt plastisk. Det visade sig att WS_2och MoS_2 kraftigt sänkte friktionskoefficienten under torra förhållanden genom att agera som en tunn skyddande-smörjfilm. h-BN presterade dåligt och ökade friktionskoefficienten. I vattenblandning lyckades inget av pulverna minska friktionskoefficienten eftersom partiklarna inte interagerade med ytorna. De testade fasta smörjmedlen bör vidare testas som beläggningar eftersom de fungerade som dessa under torra förhållanden.

Acknowledgements

Throughout the course of this thesis I have been supported by several people. The people i want to thank are:

- Pavel Krakhmalev, my supervisor at Karlstad University who has guided me through the whole project. We have had great discussions about the content of my work.
- Mikael Fallqvist, my co-supervisor at Karlstad University who also has supported and guided me through the project. Helping me with the tribotests as well as great and fun discussions.
- Henrik Svärd, my supervisor at Invecon AB for letting me do this thesis through your company and hosting me at your office.
- Peter Platell, CEO at RANOTOR for providing me with the project, great discussions and funding. You were always available and had answers to my questions.
- Rasmus Grip, CTO at RANOTOR for always being available and supporting me throughout the thesis. Your great humor and liveliness as well as technical knowledge about the product.
- Lukas Nilsson, my fellow thesis worker at Invencon for very constructive discussions about the thesis.

Table of content

1. Introduction

Energy efficiency is one of our times greatest obstacles, with greenhouse gasses and other pollutants contributing to global warming. The industry- and electricity sector emitted 48% of all the GHGs in the USA in 2021 [1]. Large amounts of the energy in both sectors comes from burning fossil fuels. With the increasing demand of energy for industrial purposes in combination with the rising price of electricity, the industry has to improve on energy efficiency in order to reduce costs and to limit their GHGs emissions.

Jouhara et al. [2] states in their article that the industrial sector stands for 33% of the global GHGs emissions, and that around 70% of the energy consumption in this sector is for heat. Especially heating, due to thermal processes, results in large amounts of waste heat, in some cases even up to 50% causing massive amounts of energy to be wasted. This raises the question of using waste heat recovery systems to take advantage of this energy thus becoming more energy efficient and sustainable. However using a waste heat recovery system can be expensive and are also characterized by their efficiency.

There are several waste heat recovery systems on the market but the specific one in this thesis focuses on extracting electricity from waste heat through a high temperature steam engine. Unlike older, low efficient steam engines used way back in the early days of industry, this one has a much higher efficiency. In collaboration with Invencon AB and their customer RANOTOR who develops this system, the focus of this thesis is to minimize heat loss and increase the lifespan by reducing friction inside the expander.

1.1 Research question

- How does the introduction of a solid lubricant in powder form affect the coefficient of friction in a steel-on-steel contact compared to non-lubricated conditions?
- How do the friction-reducing properties of the powder vary as an additive in different suspensions?
- What are the underlying mechanisms responsible for the reduced coefficient of friction?

Chosen solid lubricants for testing in this thesis are:

- Hexagonal boron nitride
- Tungsten disulfide
- Molybdenum disulfide

Delimitations were discussed with both RANOTOR and supervisors and agreed on. Friction tests will be tested at room temperature, in dry conditions and wet conditions (suspensions). No study or tests will be conducted to determine whether the particles in fact can travel with the medium throughout the engine.

1.2 Literature study

In this thesis three separate literature studies were conducted. One for each of the three additives chosen.

The methodology for each review consists of analyzing and collecting information from quantitative studies as well as qualitative studies. Quantitative studies were analyzed to gather statistical results of the coefficient of friction, derived from experiments. Qualitative studies were analyzed to gather information of how the solid lubricants yielded the results that they did in the quantitative studies.

1.3 Tribology

Tribology is the science of friction, wear and lubrication during contact between two surfaces in relative motion. The underlying mechanisms and parameters that characterize the type of contact as well as wear are difficult to predict since they vary vastly depending on current conditions. This is why new applications in the field of tribology need to be physically tested and thoroughly examined to collect empirical data. Mentioned above, many parameters

influence how two surfaces interact with each other, these parameters are included in the three main groups: friction, wear and lubrication. Key parameters that affect the tribological effects are friction coefficient (COF), wear rate, contact pressure, sliding speed, adhesion force, surface roughness, lubricant viscosity, lubricant film thickness and mechanical properties such as hardness of the material.

Tribology is used in a wide range of industries, most notable in the automotive industry. Today internal combustion engines stand for the majority of the market in this field because of its performance, reliability and versatility [3]. However the engine has some significant drawbacks, both thermal and mechanical efficiencies are low, and much of the fuel's energy is converted into heat loss due to friction inside the engine. At the same time the combustion engine has a negative impact on the environment since it contributes to pollution and the usage of fossil fuels. The main goal of tribology in the field of automotives is to reduce friction and wear in all of the moving components inside the engine. With further improvements and research the reduction of friction and wear will yield the benefits of reduced fuel consumption, reduced maintenance and increase of power output [3].

1.4 Friction

Friction is the force that opposes motion between two surfaces in contact. In simple terms it can be described as the resistance of motion. The coefficient of friction between two surfaces is calculated by dividing the friction force with the normal load as seen in Eq. 1 below.

$$\mu = \frac{F_f}{F_N} \quad (1)$$

Friction enables us to walk without slipping, grip in our tyres and also makes it possible to write with pencils, however in some cases friction can be disadvantageous as it produces heat, enables wear and reduces energy efficiency. In applications such as engines it is desirable to have a low coefficient of friction, reducing energy loss in the form of heat.

In the field of tribology the coefficient of friction is divided into three main components which are [4]:

- Adhesive component (μ_a) - chemical attraction
- Ploughing component (μ_p) - deformation by ploughing
- Topography deformation (μ_d) - deformation by asperities

The adhesive component of friction arises from atomic attraction, these attractions can be divided into physisorption and chemisorption. In physisorption the main cause of surfaces sticking to one another is the intermolecular forces developing between them in the form of Van der Waals bondings. Chemisorption is when a chemical reaction between the two surfaces takes place and creates new molecular bonds. A good adhesion between two surfaces translates to an increase of friction since new molecular bondings have to be broken and surfaces have to be sheared. In figure 1, an illustration of how the surface can shear during an adhesive contact.

a) No tangential force movement

b) Elastic/plastic deformation

c) Microsliding due to plastic deformation of contact junctures

d) Contact junctures are sheared off [4]

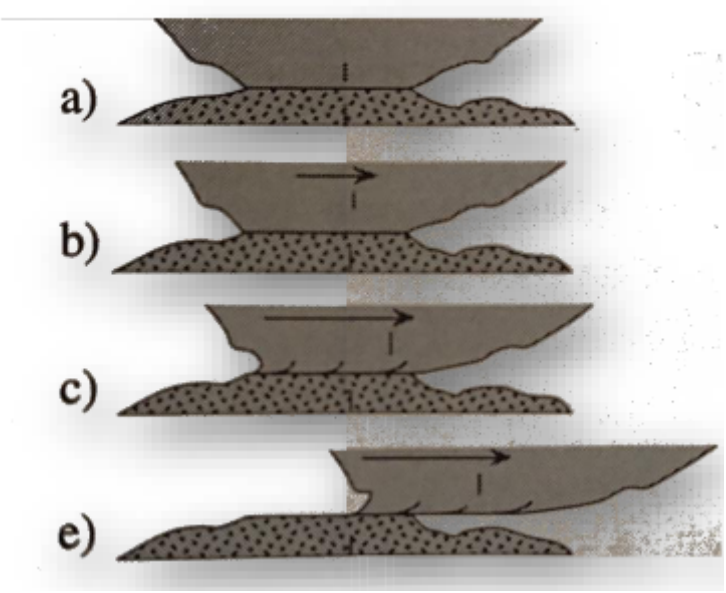

Figure 1. Shearing of a surface during an adhesive contact [4].

The ploughing part of friction occurs when asperities and irregularities from a harder surface dig or plough through the opposing softer surface. This can unfold in a couple of ways, the three most common are [4]:

- Micro cutting - Chip formation
- Micro ploughing - side flow of material
- Wedge formation

The component of topography deformation is often included into the ploughing component since both are heavily dependent on surface roughness and shape of asperities. During topography deformation, asperties and other irregularities are plastically deformed thus increasing the generated friction.

1.5 Wear

The term wear is often used in a tribological context and it is referring to “loss of material” or “removal of material”. In layman terms the phares wear is defined by the destruction of a surface, this is not the case as it is simply referring to actual loss of material. Wear is usually divided into two main categories:

- Sliding wear
  - Adhesion
- Wear by hard particles
  - Abrasion
  - Erosion

Sliding wear often results in ductile or brittle fractures which are caused by adhesion, looking at figure 2, characteristics of how these two types of wear usually appear can be seen. A ductile fracture is defined by the shear of material whilst a brittle fracture can crack or chip.

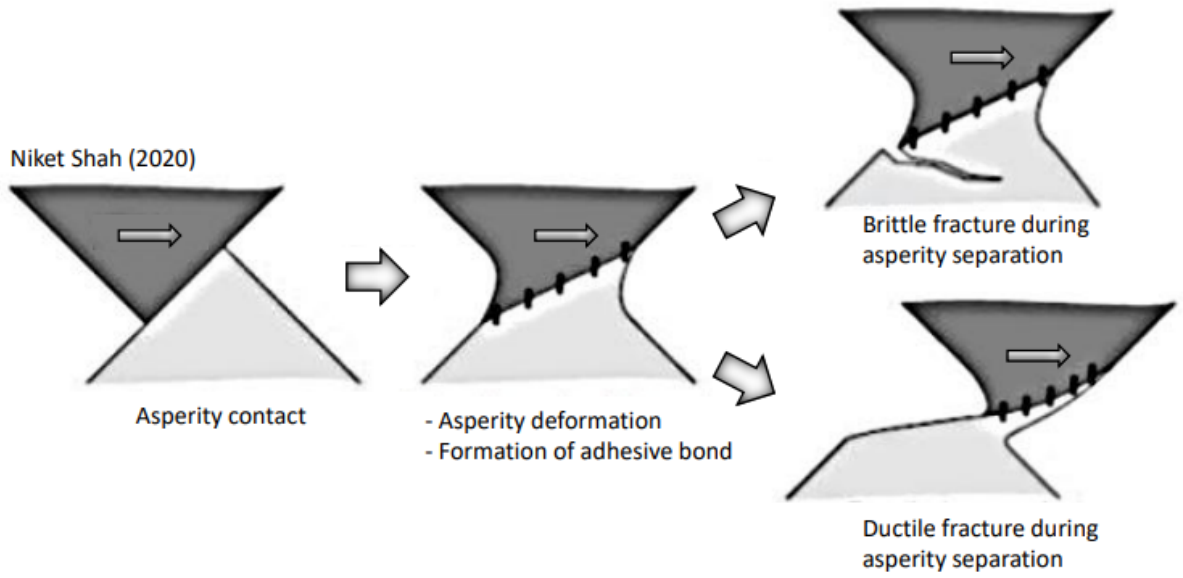

Figure 2. An illustration of a brittle fracture and ductile fracture during sliding wear [5].

Sliding wear is heavily dependent on normal load and sliding velocity, looking at the wear map in figure 3, it can be seen that the most severe type of damage is at high loads during fast velocity. The high velocity in combination with high load creates high interface temperatures which further increases the amount of wear obtained. The wear map can be applied to any tribological contact, most commonly in steel contacts.

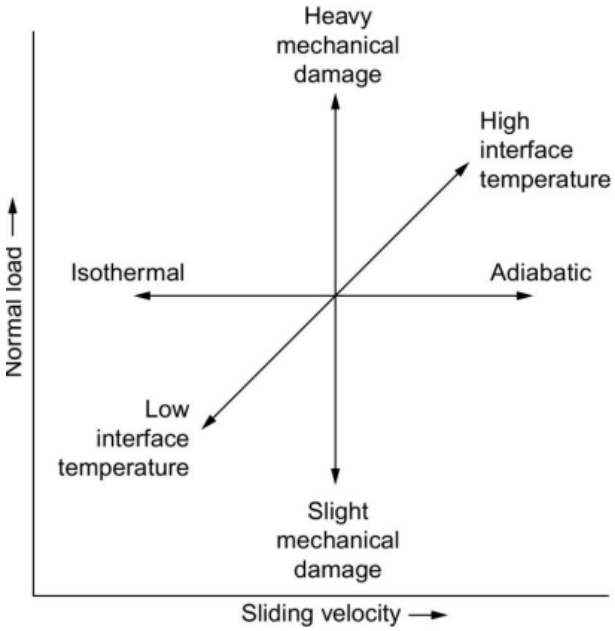

Figure 3. Wear map [5].

When dealing with wear by hard particles, the two main mechanisms are erosion and abrasion. Abrasion is built upon two main categories which are two-body abrasion (sliding abrasion) and three-body abrasion (rolling abrasion). A simple illustration of these can be seen in figure 4 (a) and b). Erosion is when particles are hitting a surface with an angle, thus causing wear, an illustration of this can also be seen in figure 4 (c).

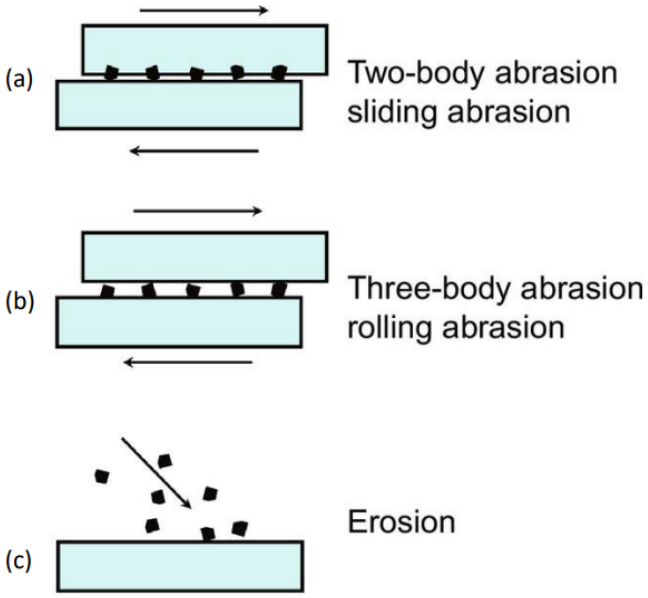

Figure 4. (a) two-body abrasion, (b) three-body abrasion, (c) erosion [6].

The wear equation is the same for both of these types of wear and follows Archard's wear equation seen in Eq.2:

$$Q = \frac{KW}{H} \quad (2)$$

Q = Worn volume per unit sliding distance
K = Wear koefficient (dimensionless)
W = Normal Load
H = Hardness of the softer material.

1.6 Lubricants

Lubricants in all of its forms are used in a tribological sense to reduce friction and wear between two surfaces. Benefits of using lubricants are decreased friction, decreased wear, cooling and corrosion resistance depending on what kind of lubricant is used. Common lubricants are oil, grease, water and solid lubricants. For a lubricant to act as intended, the lubricant must be of a layer with lower friction than both of the surfaces mated against each other. When using liquid lubrication the two surfaces follow three different regimes of lubrication which can be seen in figure 5.
Either the surfaces are fully separated by the lubricant which is named hydrodynamic lubrication, or they are partially separated which is called boundary lubrication. There is

however a third regime which is a mix of these two regimes, the surfaces are not totally separated but not enough partially separated to be classified as boundary lubrication. This regime is called mixed lubrication, some asperities are in contact which divides the load between themself and the lubricant enhancing the friction coefficient.

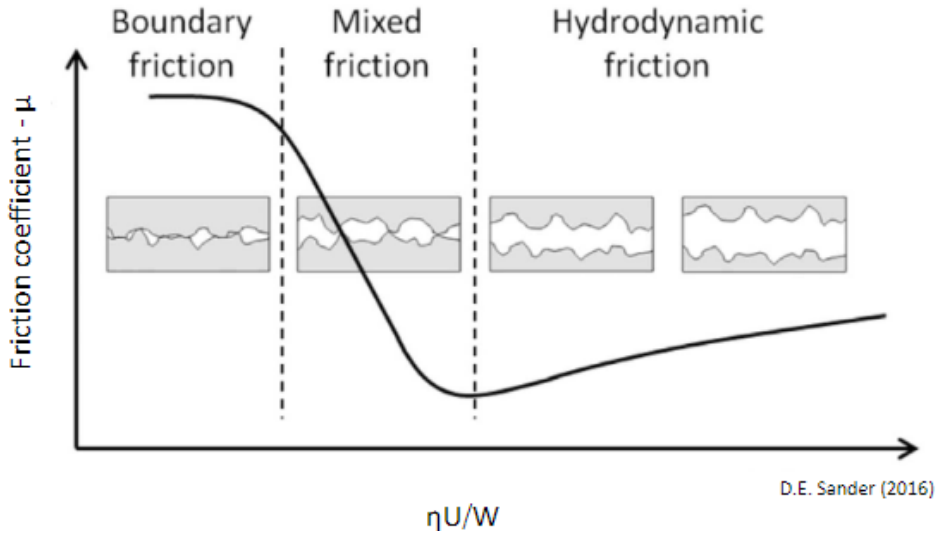

Figure 5. Stribeck curve [7].

It can be seen in figure 5. that the lowest coefficient of friction can be obtained by being on the very edge of mixed friction to hydrodynamic friction. The Y-axis represents the coefficient of friction (COF) and the X-axis is the dimensionless hersey's number which is represented by η = dynamic viscosity times U = fluid velocity (entrainment speed) divided by W = normal load per length of the tribo-contact.

1.7 The Ranotor engine

Ranotor has developed a high temperature modern steam engine that follows the Rankine steam power cycle, which is one of the most efficient ways of recovering industrial waste heat [8]. The Rankine cycle is a thermodynamic process which is used to explain the process of extracting mechanical work from a fluid while it travels through a heat generator and heat sink. Simplified, the cycle relies on a working medium, often water, is turned into steam through the addition of heat creating a high temperature, high pressure steam. It is then passed through an expander, often a turbine or piston, the steam is condensed back to a fluid and waste heat is rejected before the fluid re-enters the system thus completing the cycle. The steps of the rankine cycle and temperature-entropy graph can be seen in figure 6.

The Rankine cycle can be divided into four stages:

- 1-2 Fluid is pressurized from low to high pressure, this is called an isotropic compression.
- 2-3 Heating of the liquid occurs in a steam generator/boiler
- 3-4 Isentropic expansion in an expander, converting heat into mechanical work.
- 4-1 Constant pressure heat rejection in a condenser.

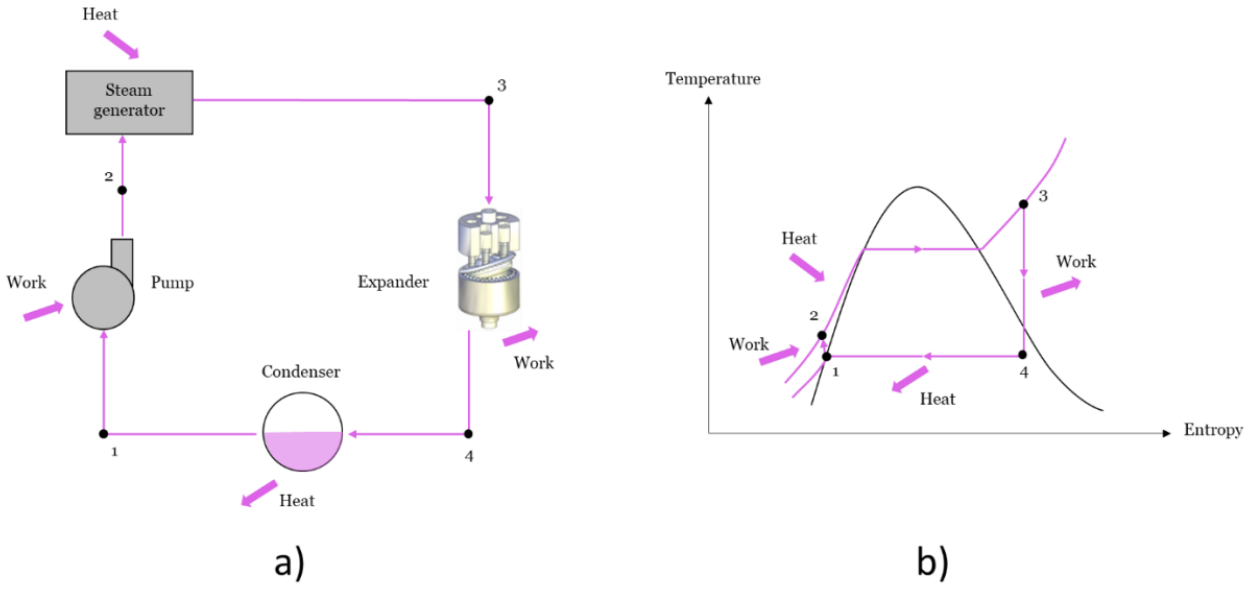

Figure 6. a) is a simplification of the RANTOR steam engine and b) is a temperature-entropy graph of the rankine cycle [9] (with permission from author).

In figure 7 the expander which is used to convert the high pressurized steam to mechanical work in the RANOTOR engine can be seen along with the main parts. Additionally to the piston, there are piston rings which are put in place to make a tight seal so that no high pressure steam escapes into the engine block causing efficiency loss. The contact areas of interest in this thesis is where the reduction of friction matters the most. The surface in the expander where this is the most crucial is between the piston rings and the cylinder block wall as well as the piston itself and the cylinder block wall.

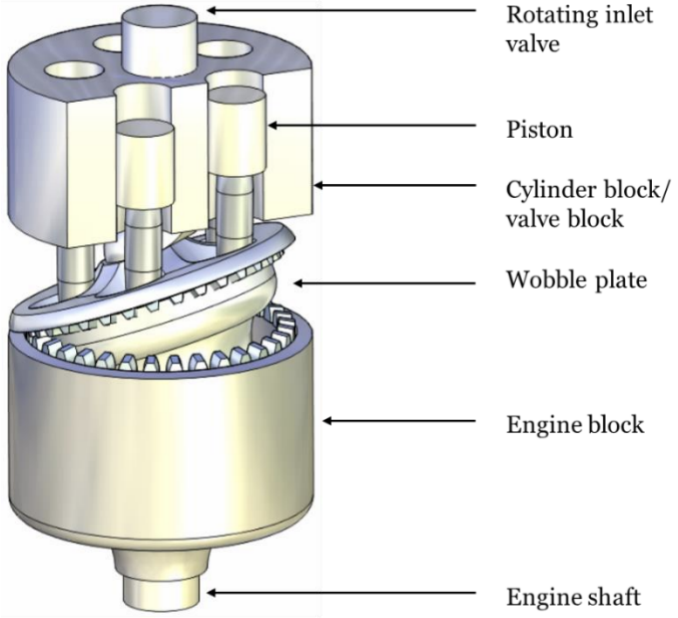

Figure 7. 3D model of the axial piston expander used in the RANOTOR engine [9].

1.8 Hexagonal Boron nitride

Boron nitride is a compound which consists of Boron and Nitride and is referred to as Boron nitride (BN). Boron nitride exists in several forms depending on what type of crystalline structure the ceramic is based on. The three most common Boron nitride structures are: Hexagonal boron nitride (h-BN), amorphous boron nitride (a-BN) and cubic boron nitride (c-BN). h-BN is the most stable form of BN in terms of thermal and chemical resistance [10]. This material review will focus on h-BN since it possesses the lubrication properties that are desired in this thesis.

The different structures of the boron nitride in terms of atom arrangement gives the compound varying properties. In the case of hexagonal boron nitride which has a structure very similar to graphite i.e layered hexagonal sheets which can be seen in figure 8. The boron and nitride are bonded through strong covalent bonds while the h-BN planes are bonded by weak van der Waals forces [11]. The weak van der Waal forces between the planes also explains why they slip easily which is a cause for a low coefficient of friction (COF).

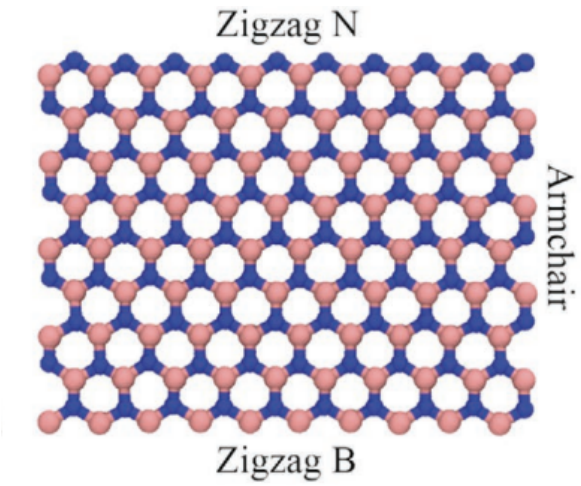

Figure 8. Atomic structure of a h-BN plane. B refers to Boron and N refers to Nitride [11].

Roy et al [11]. mentions that h-BN, like graphene, has the advantage of being malleable into nanostructures. This includes nanotubes, flakes and scrolls where nanotubes are the most common. Due to the strong covalent bonds between B and N mentioned previously, h-BN starts to decompose at 964℃ in an air medium while decomposition of the material starts at 1400℃ in a vacuum [11]. The chemical inertness of h-BN also makes it ideal as a solid lubricant since it will not react with the environment and therefore protect the bulk material underneath. In order to highlight the advantages of h-BN, it can be compared to the wonder material graphene in many aspects. One of the areas h-BN is highly prominent in is mechanical strength. h-BN sheets mechanical strength is independent of the thickness (layers) of the film which makes it highly attractive for mechanical purposes like reinforcement applications. Comparing this to graphene whose mechanical strength is dependent on thickness (layers), graphene films experience a reduction of mechanical strength of up to 30% when the amount of layers goes from 1 to 8 [11, 12]. According to Falin et al. This reduction of 30% in mechanical strength is due to some interlayer slippage between graphene sheets, even though h-BN and graphene are very similar in structure, h-BN interlayer interactions do not affect the mechanical strength in a negative manner [12].

1.8.1 Synthesis

There are three main ways to extract hexagonal boron nitride nanosheets. These three fabrication processes are CVD, borax (reaction with borax) and hydrothermal exfoliation. In this section, rather short descriptions of the process itself will be briefly explained since this is not the main subject of the thesis.

1.8.1.1 Chemical vapor deposition (CVD)

Chemical vapor deposition or in as it will be referred to in this paper, CVD, is a relatively new materials-processing technology. It is often used to synthesize thin coatings upon a substrate, bulk material or powders, where the last one mentioned is what has been acquired for this thesis.

CVD has been developed and used since the 1960's to great success. The technology has been proven to work on every, except for a handful of elements in the periodic table which shows a wide range of flexibility with this method [13].

Basics of CVD is that a precursor of gas or gasses flows into an autoclave which holds an object that is supposed to be coated with the final material. This object is heated to a specific temperature depending on what the final element should be. The heat of the object gives rise to chemical reactions both on and near the surface of the object, which then results in a deposition in the form of a thin film consisting of the desired element on the surface [13]. There are several versions of how CVD can be performed, some of them are in cold-wall reactors as well as hot-wall reactors, even the pressure can be modified to suit the chosen element.

Shi et al [14]. demonstrated in a paper, written in 2010 on how to specifically obtain a h-BN film on a polycrystalline Ni substrate. The authors [14], reportedly used a Nickel based polycrystalline surface to grow the h-BN film on. The synthesis that was carried out in this experiment was done in an APCVD which is short for atmospheric pressure chemical vapor deposition [14]. Shi et al. also reports that previous to this experiment h-BN film has typically been produced through CVD with pairs of precursor gasses such as; Boron trifluoride (BF_3) with ammonia (NH_3), boron trichloride (BCL_3) with ammonia (NH_3) and diborane (B_2H_6) with ammonia (NH_3) [14]. However this has shown to be difficult since there are several parameters that affect the outcome in terms of quality and quantity of the h-BN layers due to stoichiometric challenges and molar ratios between the precursors. To overcome these issues a single precursor borazine ($B_3N_3H_6$) carried by nitrogen (N_2) gas was pumped into the chamber where it was exposed to the polycrystalline Ni substrate. By using a singular precursor with stoichiometric relation of 1:1 B/N the problem previously stated can be solved. The temperature to initiate h-BN film growth was set to 400 ℃, usually h-BN growth happens at a wide range of temperature, but to induce a steady and controlled growth while

maintaining a high yield of high quality h-BN films, a moderate temperature was determined [14].

The growth at 400 ℃ yields a polymerization reaction which produces polyborazylene which in turn can be further dehydrogenated to form the desired h-BN. This dehydrogenation takes place during the post annealing process where the temperature is increased at a slow rate in the chamber from 400 ℃ - 1000 ℃. After heating, the specimen is kept at 1000 ℃ for an hour, the specimen is then cooled to ambient temperature where the h-BN film can be analyzed. By wet-etching the Ni substrate surface before the CVD process, the final h-BN film can be transferred to other surfaces [14].

1.8.1.2 Borax reaction

This method of producing BN and h-BN is a more traditional way of doing it compared to CVD. Through chemical reactions a precursor for h-BN is produced. Çamurlu [15] explains that a precursor for h-BN is made through the chemical reaction of urea ($CO(NH_2)_2$) and boric acid (BH_3O_3) in a mixture at elevated temperature, this produces the precursor ($HBNOH$) along with carbon dioxide and water. The precursor in this experiment was mixed with sodium carbonate (Na_2CO_3) and kept in either a nitrogen, ammonia or argon atmosphere at a temperature ranging from 700 ℃ - 1200 ℃ for a set time before h-BN is produced [15]. Results of the experiment yielded that the use of the catalyst sodium carbonate in combination with an ammonia atmosphere gives a high yield of h-BN from the precursor.

1.8.1.3 Hydrothermal exfoliation with sonication

This method when dealing with h-BN is most often used to produce h-BN nanosheets from bulk h-BN powder. A solvent is required where the powder can be mixed into, this mixture is then placed in an autoclave where temperature and pressure can easily be controlled. After the hydrothermal process is done, the specimen is placed in a sonication device for a set amount of time for the h-BN nanosheets to be exfoliated [16].

1.8.2 Application as a lubricant

In a study conducted by Ma et al. [16] the effects of using sodium -/potassium hydroxide ($NaOH/KOH$) solution during exfoliation of the powder was studied. The main focus of the study was to conclude if the hydrothermal procedure was successful and to investigate the lubrication properties of h-BN nanosheets suspended in an oil medium [16]. The study

compares h-BN powder oil suspension vs. h-BN nanosheets oil suspension vs. base oil at different wt.% in tribological aspects such as coefficient of friction and AWSD (average wear scar diameter). The tribological experiments were made in a four ball wear testing machine at different rotation speeds and loads for a set amount of time.

It was found that at 0,06 wt.% both the h-BNNS and h-BN suspensions performed the best in terms of COF, the average COF was measured to 0,08 and 0,09 respectively which can be seen in figure 9 a) [16]. Furthermore the COF was plotted as a function of time and yielded great results as both of the oil suspensions performed better than the base oil. In fact h-BN oil suspension lowered the COF by 35,2% and h-BNNS suspension lowered it by 35,7% in respect to the base oil, the plot can be seen in figure 9 b) [16]. It was also found that both of the suspensions managed to decrease the wear rate significantly.

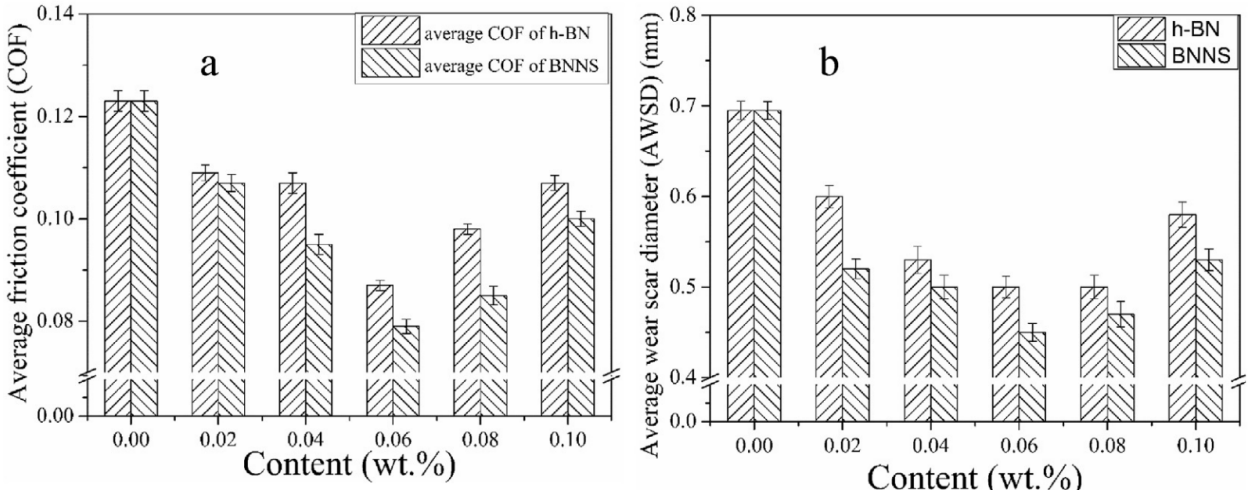

Figure 9. a) Bar chart of average COF vs. wt.% content of stated material. b) COF as a function of time, base oil vs. h-BN and h-BNNS oil suspensions [16].

The author states that the reason for h-BN and h-BNNS oil suspension effectively reduces the COF and wear is their ability to easily cover the surface and create a protective-lubricating film with a continuous supply of particles surrounding it. However the suspensions average COF is heavily dependent on wt.%, it is said that above 0,06% wt.% the medium is “over-saturated” and tends to agglomerate the particles/nanosheets which limits the suspension's ability to supply the contact area with a constant feed [16].

Hexagonal boron nitride is reportedly widely used as an additive self lubricating material in many areas, some applications where h-BN is used is in cosmetic make-ups as a slip modifier [11]. Other areas such as additives in oils used in combustion engines instead of graphite since it would oxidize and clog the engine filters. Due to it being thermally stable

and chemical inertness it is often used in high temperature and high pressure applications such as bearings. It is often used as an additive in rubbers, ceramics and alloys giving them self lubricating properties [10].

According to some vendors of h-BN powder, it can be dispersed in water to form a slurry which reduces the coefficient of friction between two surfaces. A study conducted by Abdollah et al. [17] investigated the influence on friction coefficient of h-BN powder with a particle size of 70 nm in diameter mixed with water on a steel-steel contact. The nano addative was added with a 0,1 - 0,5 vol.% to distilled water and then homogenized with an ultrasonic homogenizer. The mixture was then tested with a four-ball tribometer to acquire the appropriate data.

In figure 10 below, collected data from the experiment conducted can be seen. In figure 10 a), COF is plotted against time with data lines in different colors that represent the mixture of h-BN with water in vol.%. The graph visualizes a concentration of 1,0 vol.% improved the COF the most and in close following a concentration of 0,5 vol.%. The authors state that once the concentration exceeds 1,0 vol.% concentration the COF rises gradually and testing had to stop [17]. The reduced COF is most likely due to the mechanisms in the Stribeck curve as the vol.% affects the viscosity of the mixture. It can be seen in figure 10 b), that a concentration of 1,0 vol.% results in the nanolubricant being on the edge of the mixed region which should yield the lowest COF. While being in the mixed region regime, only a few asperties where the surface roughness is much greater, are in contact. The lubricant manages to separate most of the surfaces which gives opportunity for interlayer slippage between the h-BN nanoparticles, which is one of the reasons for low coefficient of friction as stated in section 1.8. Once the concentration was increased to 3,0 vol.% agglomeration of the nanoparticles could be seen and the regime changes from the mixed region to the hydrodynamic region thus increasing the COF [17].

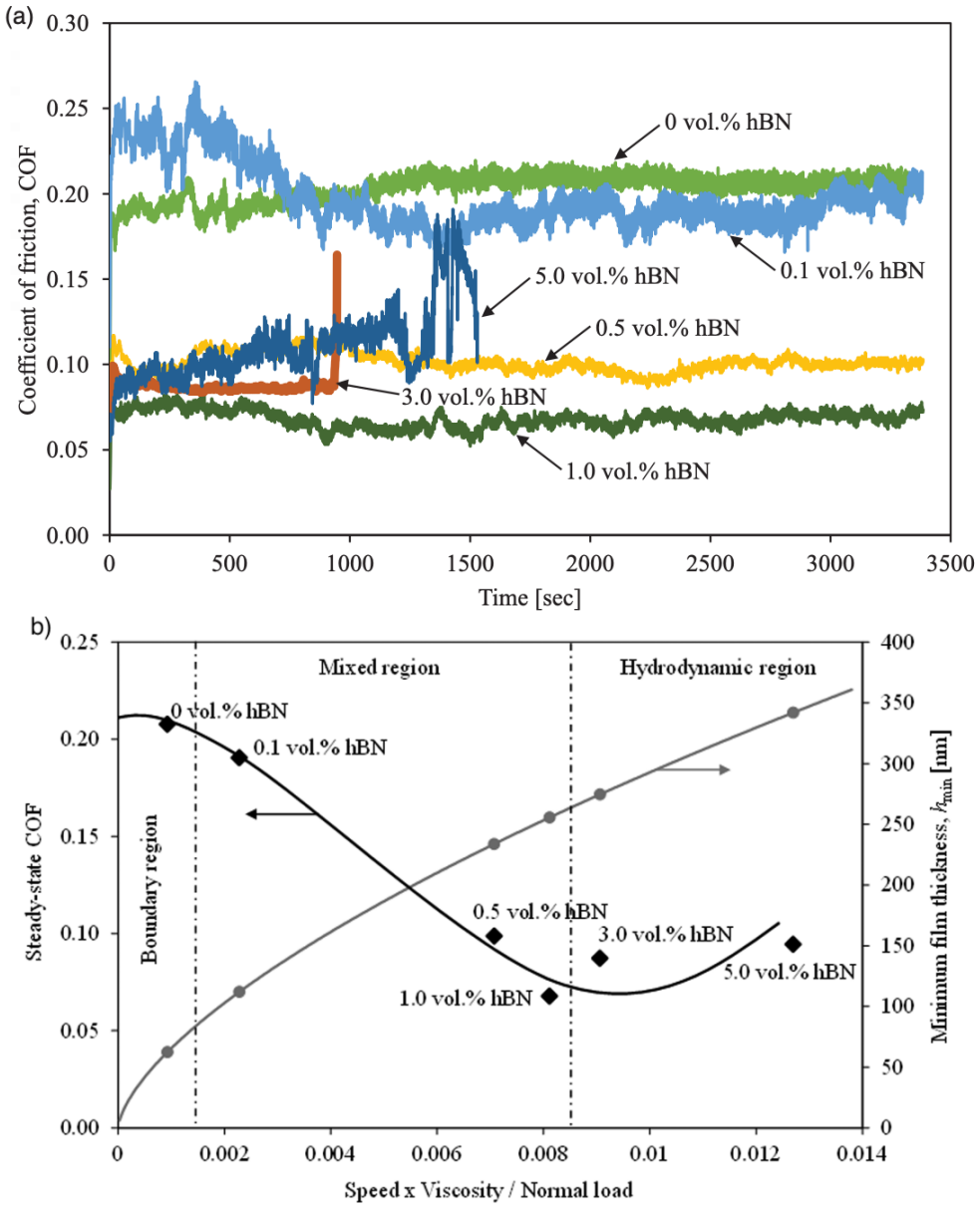

Figure 10. a) COF plotted against time. b) Stribeck curve constructed from plot a) [17].

1.9 Tungsten disulfide

Tungsten disulfide is a part of the compound group “transition metal dichalcogenides” (TMDs). Most TMDs are also a part of the group 2D-materials which refers to a crystalline structure which is stable as a single layer. TMD is recognized by its elemental build blocks and have the composition MX_2 where M is a transitional metal and X is a chalcogen like sulfur (S), selenium (Se) or tellurium (Te) [18]. TMDs have their structure in common, a layer structure where M atoms are sandwiched between two layers of X atoms.

As for the case of Tungsten disulfide (WS_2), the tungsten atom layer is sandwiched between two layers of sulfur (S). Each of the layers has a hexagonal crystalline lattice structure. W and S atoms are bonded by strong ionic-covalent bonds while the structure itself (the sandwich layers) is held together by weak Van der Waals forces similar to h-BN mentioned earlier [18]. WS_2 can be used in many applications such as batteries, photodetectors, lubricants and many more due to its inherently good electronic- and mechanical properties. Like hexagonal boron nitride, tungsten disulfide also has the advantage of being malleable into nanotubes, flakes and scrolls depending on what is suitable for the desired application.

1.9.1 Synthesis

Currently there are several synthesis process to obtain WS_2. These are commonly divided into three categories; physical, chemical and stripping methods. The different methods will be briefly explained in this section.

1.9.1.1 Physical methods

The two main methods in this category are pulsed magnetron sputtering and pulsed laser deposition (PLD). Pulsed magnetron sputtering has the advantage using fairly simple and low cost equipment while yielding a large dense coating area with good adherence. In contrast to pulsed magnetron sputtering, PLD is more costly and complex in terms of operation, however it holds the ability to be able to control the thickness of the film while maintaining a high quality [18].

In the pulse magnetron sputtering a solid material is bombarded under vacuum conditions to cause the object to sputter. Sputtering is where particles from the material are ejected due to being bombarded by high energy particles. This is why a high quality vacuum is needed for this process otherwise the ejected particles would collide with molecules in the air. The ejected particles are aimed at the substrate to induce the growth of a thin film. In the case of WS_2, the sputtering target is a cathode made of WS_2. Argon gas is passed into the vacuum chamber while a high negative cathode voltage is applied to trigger glow discharge. The WS_2 cathode's surfaces are bombarded with Ar ions under the influence of an electric field, this causes the target to sputter and eject particles that are deposited into the substrate [18].

Ding et al [18]. mentions that often when dealing with WS_2 films, it is favorable to enhance the adhesion between the film and substrate. This is done by first depositing a film of chromium (Cr) and then adding the WS_2 film.

As mentioned earlier, pulsed laser deposition (PLD) is a somewhat more expensive and complex process. The principle of PLD revolves around the usage of pulsating lasers to evaporate some areas of the target's surface which creates a high density plasma due to the rapid temperature increase in that area. The emitted plasma plume is aimed at the substrate which in contact deposits the WS_2film [18]. Ding et al [18]. has reviewed an experiment where the result of the study showed that the thickness (monolayer, multilayers) of the WS_2 film had a direct correlation to the number of incident laser pulses. This makes it possible to control the thickness of the film by controlling the previously stated.

1.9.1.2 Chemical methods

There are two common methods where WS_2 films are prepared, these are CVD and growing single WS_2 crystals with a hydrothermal method. Information about chemical vapor deposition (CVD) has already been covered previously in this paper in section 1.8.1.1, therefor the description in this section will focus more on the specifics of CVD dealing with WS_2.

There are two methods available when preparing WS_2 by CVD, the one-step and two-step method. The one-step includes direct heating of tungsten and sulfur which is transported with a carrier gas to the substrate. A common tungsten source which is used for this purpose is often tungsten trioxide (WO_3), the typical chemical reaction to form a WS_2 film by tungsten trioxide reaction looks like:

$$2WO_3 + 7S \rightarrow WS_2 + 3SO_2$$

This coating is often deposited on either a silicon, copper or quartz substrate [18].

The two-step method utilizes CVD in a somewhat different way, at first, the substrate is coated with a tungsten or tungsten compound. The substrate is then vulcanized in a CVD furnace to synthesize the WS_2 film. In this method, the initial coating is usually deposited onto the substrate's surface by pulse magnetron sputtering. Ding et al [18]. reviewed an experiment where the purpose was to see if the number of layers of the WS_2 film could be controlled by regulating the thickness of the initial tungsten coating. The experiment showed

that the number of layers indeed could be accurately controlled by the thickness. Advantages of using the two-step CVD method instead of the one-step method is that it has the ability to prepare large-scale films which is one drawback of the one-step method. However the two-step method still has some drawbacks which includes the need for high substrate temperature and expensive equipment [18].

Hydrothermal method, also referred to as a wet chemical synthesis. This particular method is great for preparing WS_2 particles with a high purity and crystallinity, on the other hand, the method lacks the ability to control the thickness of the films. To synthesize WS_2 through this method, typically a mixture of sodium tungstate dihydrate ($Na_2WO_4 \bullet 2H_2O$) and sodium sulfide (Na_2S) are dissolved in deionized water until a clear solution is achieved. The solution is heat treated in a hydrothermal reactor for a set amount of time and temperature. After the process in the reactor is finished, the solution is washed with ethanol and dehydrated so that the WS_2 particles can be collected [18].

1.9.1.3 Stripping methods

Stripping methods in its core is essentially moving a thin film or layer from a bulk material onto another surface. There are several ways this can be done but the most widely used ones are mechanical exfoliation and liquid exfoliation. Mechanical exfoliation is a very simple method of stripping thin films from bulk material, in this case WS_2. A piece of tape with good adhesion is used, it is repeatedly pressed onto the surface of the bulk material, thereby stripping it. When a thin film of the bulk material has adhered to the tape, it can then be transferred from the tape to another surface, it is however important to make sure the thin film peels off slowly from the tape to ensure good adhesion between the substrate and film. Usually the film is transferred to a substrate like silicon dioxide (SiO_2) or silicon (Si) [18]. Mechanical stripping has its advantages of being a fairly simple procedure with great results in terms of crystallinity and few defects in the film. Drawbacks with this method are its low applicability due to the reason of being difficult to peel large areas and low repetition rate [18].

The liquid exfoliation method is based on utilizing ultrasonic waves to loosen and separate the layered WS_2 through shear force and cavitation bubbles. Once the layers have been separated, the material is dispersed in a solvent. The key to being able to peel the separate layers is choosing a suitable solvent since the surface tension of WS_2 is estimated to be

somewhere around $40\,mJ\,m^{-2}$. Some typical solvent that are used in this method are ethanol, water and propanol [18]. Ding et al. [18] mentions that ammonia as a solvent, reportedly improves the stability of the suspension while also decreasing the amount of time the material has to be exposed to ultrasonic waves before being dispersed into the solvent. Liquid exfoliation is great for preparing large amounts of WS_2films, there is however no way of being able to control the thickness of the films which makes them rather non uniform in thickness. WS_2 prepared this way are not as pure as other methods which makes it less attractive.

1.9.2 Application as a lubricant

WS_2 is a known friction reduction enhancer due to its inherently weak Van der Waals bondings between layers, just as the case of h-BN. The most commercially used form of WS_2 is in a solid lubricant state, which most often is a coating or additive in a composite to increase its self lubrication properties. It is a very stable material/additive which can operate in high temperature and extreme pressure environments which makes it ideal for the aerospace industry where liquid lubricants cannot be used [18]. As for lubrication purposes in powder form, both in a medium suspension or dry powder, there have been few studies conducted and no studies have been found as to how its lubricating properties change in a water mixture.

A study performed by Wu et al [19]. was carried out to investigate the influence of WS_2 powder with two different particle sizes and concentrations in an oil medium. The two particle sizes were 2 microns and 90 nanometers at concentrations of 0,5 - 2,0 wt.% in increments of 0,5 wt.%. an extra step was also carried out to test how the lubrication properties of WS_2 changed with the addition of an ionic fluid to the oil base. Preparing each sample which contained WS_2 included the step of ultrasonically dispersing it for 10 minutes [19].

The friction tests were carried out on a four-ball friction tester. Results of the experiments concluded that an optimal wt.% of 1% for the nanoparticles and 2% for the microparticles, reduced the COF immediately at the start of testing and even more relative to the base oil the longer the test went on for up to a point. Figure 11 reflects the results of the authors [19] study.

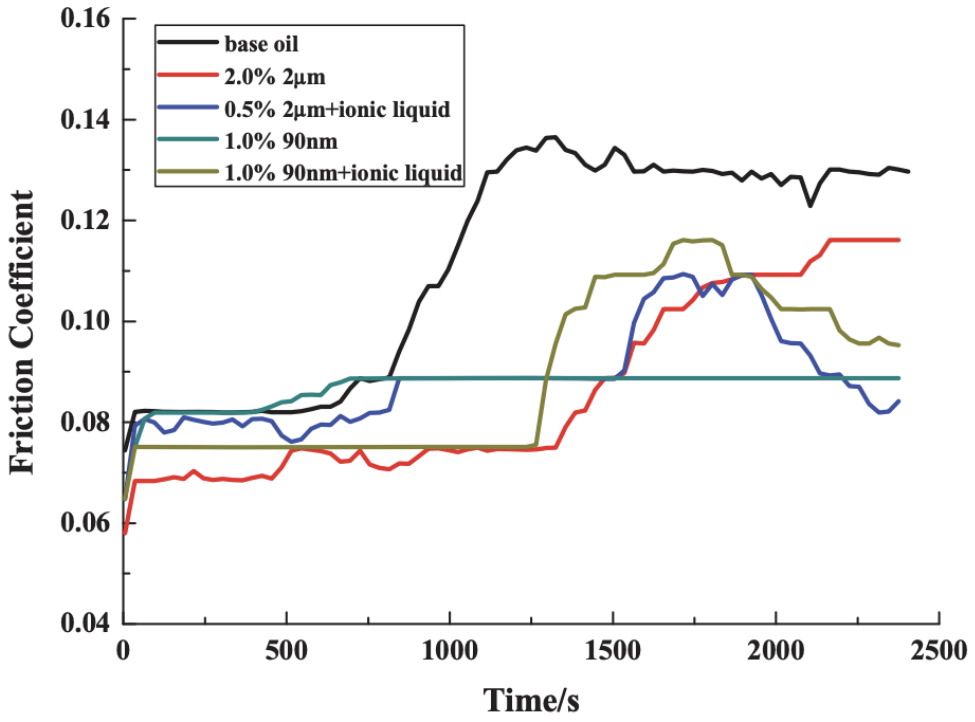

Figure 11. Comparison between the optimal wt.% of the WS_2 powder dispersed in the oil medium [19].

Another study conducted by Shi et al. [20] was carried out to determine the friction improvement of WS_2 powder added to a motor oil compared to existing standard motor oils. This experiment was also carried out in a four-ball friction tester. The authors state that the "best content for tungsten disulfide is 1% in motor oil" [20] , without further explanation. However the results of this study supports the conclusion Wu et al. [19] came to which is that the addition of WS_2 particles enhance the friction properties of the medium.

1.10 Molybdenum disulfide

Just like the previous material (tungsten disulfide), MoS_2 is also a part of the compound group "transition metal dichalcogenides" or in short TMDs. MoS_2 also happens to be of the characterization of 2D-materials. Like other TMDs and 2D-materials, as stated previously, they have their structure in common which is a layered structure. In the case of molybdenum disulfide, Mo atoms are sandwiched between two layers of sulfide ions. Within the layers, atoms are bonded together by strong covalent bonds and the adjacent layers are bonded together by weak van der Waals forces which is essential for the material to have good lubrication properties in bulk form [21]. The author states that the material has been observed to have a shear strength against a normal load of 24,6 MPa, this is a critical

parameter when dealing with solid lubricants since its main purpose is to lower the friction and enhance sliding [21]. MoS_2 exists in three different crystalline structures, the different structures are trigonal, hexagonal and rhombohedral where the hexagonal structure has been shown to be the most stable one. In figure 12 a), a top down view and side view of hexagonal MoS_2 can be seen in b).

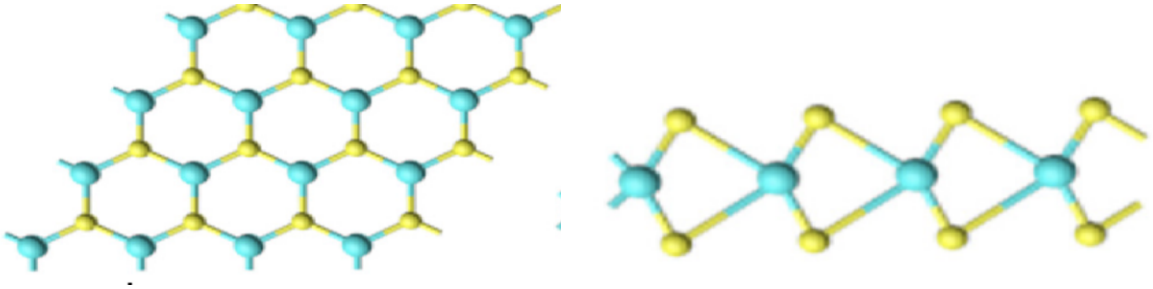

Figure 12. a to the left, b to the right. Crystalline structure of hexagonal MoS_2. Fig a is a top down view, fig b is a side view [21].

Due to the anisotropic system of the structure of MoS_2 , it opens up for a widely useful material in many application areas such as electronic conductivity and lubricants.

1.10.1 Synthesis

There are many ways to synthesize MoS_2, depending on what nanostructure is desired. Like other TMDs, MoS_2can be fabricated into nanotubes and nanosheets. The synthesis processes are divided into two main groups dependent on what processes take place. The two different synthesis groups are physical and chemical methods. Physical methods often include high-energy methods such as sputtering, laser ablation and microwave plasma. Chemical methods like CVD, solvothermal and decomposition relies on chemical reactions. Drawbacks of using physical methods are that the desired nanostructures are infrequent and often accumulate at certain spots on the surface. This can cause a reduction of surface area and decrease or even be detrimental to the function of the intended application [22]. There are many techniques used to synthesis MoS_2 nanostructures, most of these have been stated earlier and are of similar character thus they will not be further elaborated in this section.

1.10.2 Application as a lubricant

As stated previously MoS_2shares the atomic sandwich structure which is easily sheard. This is the main reason why MoS_2 has a low COF and is useful in such applications. Due to good chemical inertness, relatively high working temperature and can withstand extreme pressures which makes it a very attractive material to use, both in the form of coatings and as an additive in oils. MoS_2 is a popular choice in space-engineering since liquid lubricants will not meet the demands of the working conditions of space. In those conditions standard liquid lubricants would evaporate and even decompose. MoS_2 is used as a coating or additive in a compound in ball bearings and slip rings in space applications. The lubricity properties of MoS_2 are known to decline when in humid environments, this can however be offset by the addition of titanium to milden the effects [21]. $MoS_2$is also used as a coating for bullets, this is to ensure that the bullet travels through the gun barrel effectively. This lubricant is often added to aviation engine oil to enhance the tribological effects.

Farsadi et al. [23] published a paper about the influence of nanocomposites as an additive in oil to modify the friction. One of the materials the authors [23], conducted extensive experiments on was molybdenum disulfide and with the addition of functionalized reduced graphene oxide (FrGO). The goal of the study was to evaluate how the addition of these nanocomposites would affect friction and wear in an oil medium.

Dispersions of oil based mediums with the additives were produced and then tested in a four-ball friction machine to gather the data. Four different wt.% dispersions was used with only adding MoS_2 powder with an average particle size of 50 nm. Same wt.% was used when testing dispersions containing both $MoS_2$and FrGO [23].

Results of the friction part of the study can be seen in figure 13 below. The authors [23] state that a 0,3 wt.% of MoS_2 yielded the lowest COF to the reference base oil by a reduction of 12,4%. As for the table to the right in figure 13, a base oil was used and then the 0,3 wt.% oil was used when introducing FrGO as an additive [23]. It was determined that an addition of 0,8 wt.% FrGO enhances the already reduced friction of the MoS_2 base oil even more to 15,8%. The addition of FrGO to in the mixture is thought to have a positive effect hindering the MoS_2particles to agglomerate which is a known problem when dispersing it in oil [23].

Coefficient of friction (CoF) in a 1-hour steady state at ambient temperature.

Sample	Average coefficient of friction	Difference
Base oil	0.076734	Benchmark
MoS_2 (0.1 wt%)	0.070099	−8.6%
MoS_2 (0.2 wt%)	0.069853	−8.9%
MoS_2 (0.3 wt%)	0.067196	−12.4%
MoS_2 (0.4 wt%)	0.078675	−2.5%

Coefficient of Friction (CoF) in a 1-hour steady state at ambient temperature.

Sample	Average friction coefficient	Difference
Base oil	0.076734	Benchmark
MoS_2-based FrGO (0.4 wt%)	0.070555	−8%
MoS_2-based FrGO (0.6 wt%)	0.069794	−9%
MoS_2-based FrGO (0.8 wt%)	0.064598	−15.8%
MoS_2-based FrGO (1 wt%)	0.067249	−12.3%

Figure 13. Tables of the achieved results through friction testing in oil suspension [23].

Due to the problem with agglomeration in oil medium, MoS_2 powder can be used under dry conditions as a solid lubricant, it forms a low-shear, adherent film on metal surfaces which yields a low friction coefficient due to the sandwich structure and its low shear-strength, which has been covered earlier.

2. Materials and methods

2.1 Materials

The base material (pin and plate) that will be used during friction testing have been determined to be stainless steel 304. This is mostly due to the request of Ranotor because of its corrosion resistance and the easy accessibility. SS304 plates have been acquired from the workshop at KAU and plasma cut to rectangular dimensions 15x7,5 cm to fit the $Forceboard^{TM}$, which is the friction tester equipment. As for the pins, they were acquired through a commercial hardware store. The pins bought had an end radius of 10,9 mm (more on this in section 3.1.1), a diameter of 12 mm and length of 50 mm. The attachment point for the $Forceboard^{TM}$ requires a 6 mm or less diameter to be able to fit tightly, which is why the workshop at KAU had to lathe the ends of the rods. The final product of the rod can be seen in figure 14 below.

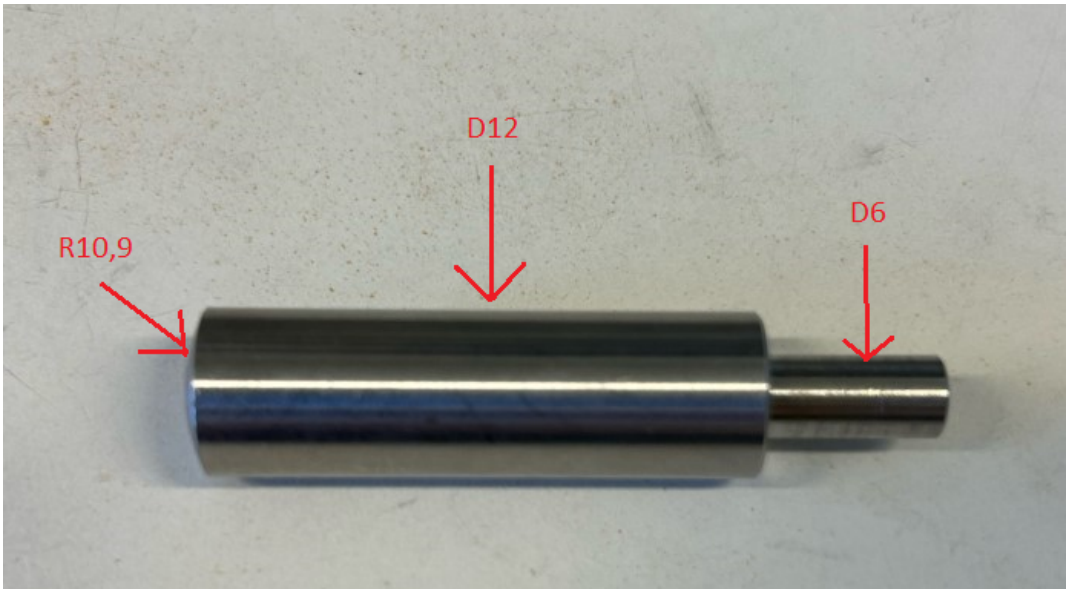

Figure 14. Final product of the pins used in testing.

2.1.1 Lubricants

The solid lubricants had to be determined early on in the thesis as to minimize the risk of delays and other complications during shipping. The lubricants had to fulfill two main properties to be a contender. The properties were;

- Working temperature 20-450 ℃ (does not have to tolerate 450 ℃)

- Withstand pressure of up to 250 bars

With the help of supervisors at KAU and a pre-literature study, three solid lubricants in powder form were selected. The selected lubricants are widely known to be used as solid lubricants in several fields and are often referred to as “graphene like materials” by vendors. The three lubricants and some of their important properties can be seen in table 1.

Throughout the thesis a more advanced and comprehensive literature study was built upon the previous pre-study regarding the selected lubricants.

Table 1. Properties of the chosen solid lubricants.

	Particle size (μm)	Working temperature @air	Load capacity (kbar)
Molybdenum disulfide powder[1] (MoS_2)	1,5	$\leq$ 400 ℃	$\approx 17,2$
Tungsten disulfide powder[2] (WS_2)	0,58	$-270℃ \leq x \leq 650℃$	$\approx 20,7$
Hexagonal boron nitride powder[3] (h-BN)	10	$\leq 1000℃$	$\approx 10,3$

[1] https://lowerfriction.com/dry-solid-lubricant-powders/molybdenum-disulfide-mos2-powder/
[2] https://lowerfriction.com/dry-solid-lubricant-powders/tungsten-disulfide-ws2-powder/
[3] https://lowerfriction.com/dry-solid-lubricant-powders/hexagonal-boron-nitride-hbn-powder/

2.2 Hertzian contact pressure and shear strength

For tribological tests like this, there is a maximum contact pressure that has to be considered as the aim of the test is to determine the friction constant between the sphere and plane with the addition of solid lubricants. The maximum shear stress allowed during testing can be obtained by analyzing the maximum contact pressure gathered by calculations.

Hertzian contact theory handles the contact between two solid objects, in this case a sphere and a plane. The theory includes certain assumptions, if these assumptions are not met, the contact would be considered a non-hertzian contact. As to not complicate the contact mechanics further the following assumptions will be considered:

i. The strains are small and within the elastic limits.
ii. Each body can be considered an elastic half-space (the contact area is much smaller than the characteristic radius of the body).
iii. The surfaces are continuous and non-conforming.
iiii. Friction during contact is disregarded [24].

From this, contact area, indentation depth, contact stresses, contact pressure and shear stresses can be calculated given the correct parameters which is needed to correctly design the tribological tests in this thesis.

Tribo-pair selected for this study is self-mated stainless steel 304 as a reference regarding friction. In table 2, key mechanical properties for choosing loads and radius of the indenter are listed for stainless steel 304.

Table 2. Mechanical properties of SS304.

	Poisson's ratio	Modulus of elasticity	Tensile strength, yield (σ_y)	Yield strength, shear (60% of TSY)	Tensile strength, ultimate (σ_B)	Ultimate shear strength (75% of TSU)
304 (annealed bar)	0,29	193 GPa	235 MPa	141 MPa	640 MPa	480 MPa

The object of interest in designing a sliding test like this is to make sure that both the indenter and plane are not critically damaged during testing. During the experiment due to the sliding motion, both plane and indenter will encounter shearing stresses which is why parameters such as radius of the indenter and load has to be evaluated. Looking at table 2 first row, if the shear stress exceeds 141 MPa, the steel will start to plastically deform due to shear stress. If the shear stress exceeds 480 MPa the material will cause a sliding failure which is classed as critical.

According to Genov [25] who in November 2020 revisited the well known system of converting yield and ultimate strength to shear strength. The author [25], states that the rule-of-thumb i.e.

$$\tau_{sh} = 0,6 * \sigma_y \quad (3)$$

$$\tau_{sh} = 0,6 * \sigma_B \quad (4)$$

is somewhat misleading in the case of expression 3 (Eq. 3). It turns out that in general this is a vast underestimate compared to the experimental obtained YSS which often leads to over dimensioned parts with higher material costs than needed. In figure 15 there are three lines representing the rule-of-thumb, a better fit line and a reference line. The two axes are τ_{sh} (yield shear strength) vs. σ_y (tensile strength, yield). As can be seen in figure 15, most of the materials experimentally obtained yield shear strength is way higher than what the rule-of-thumb predicts. Genov [25] states that after further analysis, 95% of all 1885 compiled τ_{sh} values through experimental testing, lie above the $\tau_{sh} = 0,6 * \sigma_y$ line in figure 15. The green line in the graph ($\tau_{sh} = 0,65 * \sigma_y + 68$) represents the best fit line, even though it fits the data entries better in a linear way, it would not be viable to use when

configuring a sliding test. The reason why the best fit line would not be viable is because it would overestimate the yield shear strength in 50% of the cases [25]. However Genov [25] revises the original rule-of-thumb and describes that by increasing the original coefficient of 0,6 to 0,65, 91% of the experimentally obtained yield shear strength values would still lie above that line.

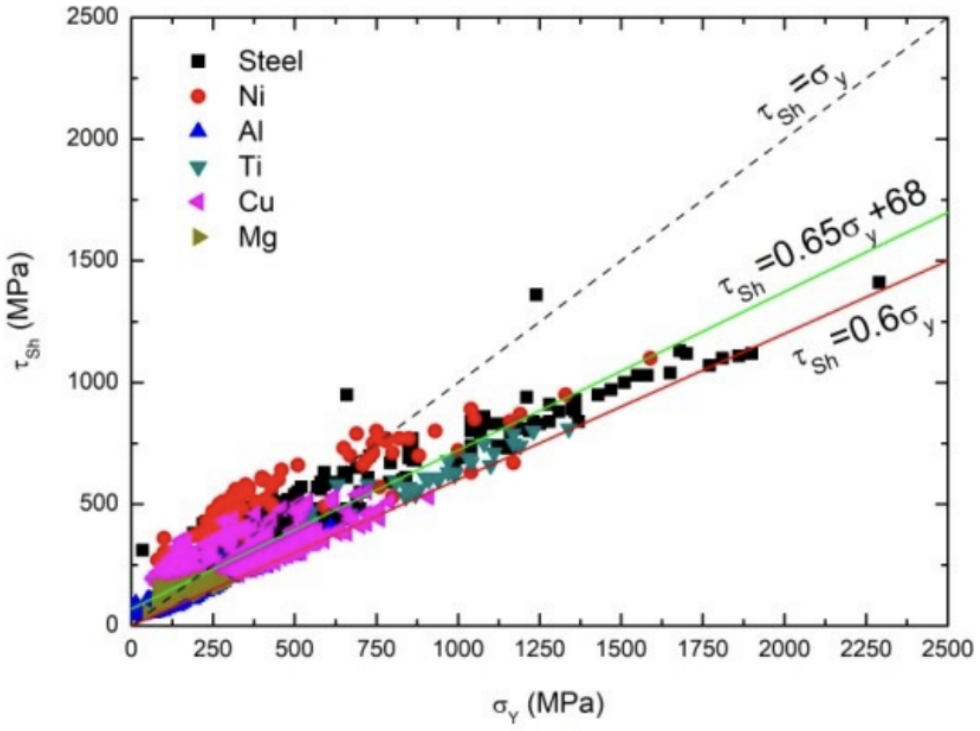

Figure 15. A plot of the measured τ_{sh} Values vs. σ_y along with three lines. Red line is the well known, rule-of-thumb $\tau_{sh} = 0,6 * \sigma_y$, green line is the best-fit-line ($\tau_{sh} = 0,65 * \sigma_y + 68$) and the dotted line $\tau_{sh} = \sigma_y$ is a reference line [25].

In the case of expression 4 (Eq.4) using ultimate tensile strength, the spread of the data points seen in figure 16 is significantly smaller. Genov [25] mentions that ultimate tensile strength clearly scales better with the rule-of-thumb than yield strength. The estimation of ultimate shear strength faces the same problem as yield shear strength. By using the rule-of-thumb, 51% of the points lie above the line and 49% below the line which makes the expression invalid since it overestimates 49% of the points. The author [25] revises the rule-of-thumb and state that the best fit line is $\tau_{sh} = 0,61 * \sigma_B + 2,4$, however it is not shown in figure 16, since it is so similar to $\tau_{sh} = 0,6 * \sigma_B$. Stating previously that using the best fit line or a very similar equation results in overestimating about 50% of the materials shear strengths which is not viable when designing a test. However, by slightly modifying the

already in place rule-of-thumb equation to $\tau_{sh} = 0,6 * \sigma_B - 25$ [25], 93% of the data points lie above the line which is acceptable.

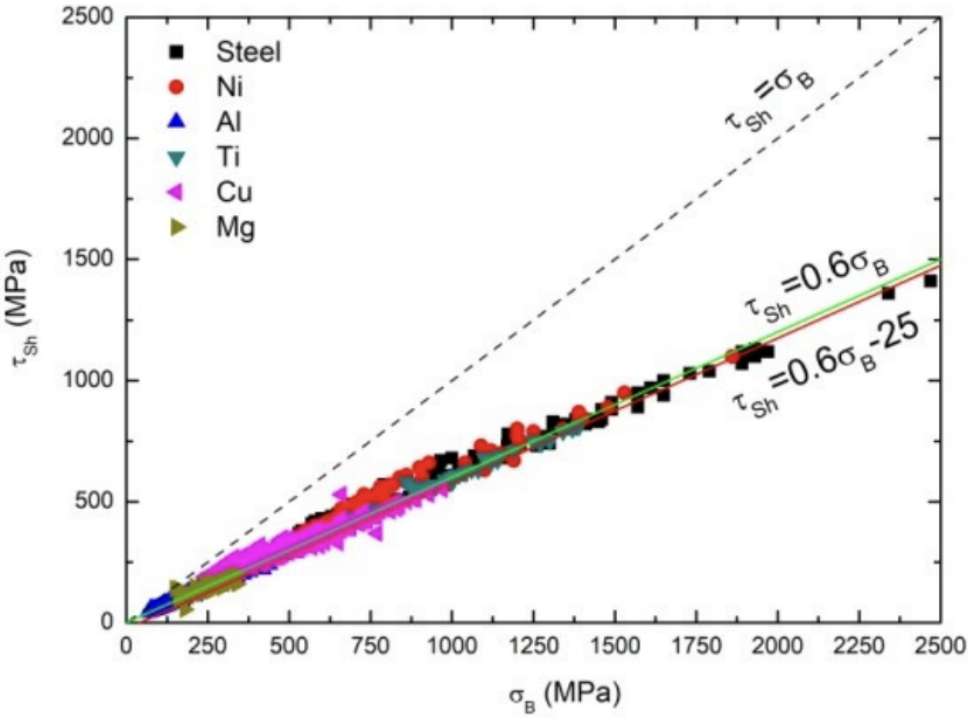

Figure 16. A plot of the measured τ_{sh} Values vs. σ_B along with three lines. Green line is the well known, rule-of-thumb $\tau_{sh} = 0,6 * \sigma_B$, red line is the modified rule-of-thumb to include more material ($\tau_{sh} = 0,6 * \sigma_B - 25$) and the dotted line $\tau_{sh} = \sigma_y$ is a reference line [25].

Table 3 is the revised material sheet from table 2, taking the findings above into consideration. In conclusion the lower limit of yield shear strength has been increased while the ultimate shear strength has decreased. As a side note, the ultimate shear strength of stainless steel 304 has been measured up to 400 MPa [26]. As to why the USS does not scale too well with this material is unknown, both of the revised equations are still valid and will be used.

Table 3. Revised material sheet.

	Poisson's ratio	Modulus of elasticity	Tensile strength, yield (σ_y)	Yield strength, shear $\tau_{sh} = 0,65 * \sigma_y$	Tensile strength, ultimate (σ_B)	Ultimate shear strength $\tau_{sh} = 0,6 * \sigma_B - 25$
304 (annealed bar)	0,29	193 GPa	235 MPa	152,75 MPa	640 MPa	359 MPa

2.3 Shear stress calculation

In order to determine the shear stress that occurs during a hertzian contact an online hertzian contact calculator was used [27]. The calculator was cross-checked through handmade calculation using hertzian theory to make sure it provided accurate results.

The calculator solves for maximum shear stress by utilizing standard hertzian spherical contact and principal stress -theory with equations accordingly figure 17 below [27]:

Principal stress (σ_x)

$$\sigma_x = -p_{max}\left[(1-\left|\frac{z}{a}\right|\tan^{-1}\frac{1}{|z/a|})(1+v)-\frac{1}{2(1+\frac{z^2}{a^2})}\right]$$

Principal stress (σ_y)

$$\sigma_y = -p_{max}\left[(1-\left|\frac{z}{a}\right|\tan^{-1}\frac{1}{|z/a|})(1+v)-\frac{1}{2(1+\frac{z^2}{a^2})}\right]$$

Principal stress (σ_z)

$$\sigma_z = \frac{-p_{max}}{1+\frac{z^2}{a^2}}$$

Maximum shear stress (τ_{max})

$$\tau_{max} = \frac{\sigma_x - \sigma_z}{2} = \frac{\sigma_y - \sigma_z}{2}$$

Figure 17. Principle stress and maximum shear stress formulas used by the online calculator [27].

The equations used for cross-validating the calculator in terms of maximum pressure in a hertzian manner were Eq.5, Eq.6 and Eq.7:

$$F = \frac{4}{3}E^{\star}R^{1/2}d^{3/2} \quad (5)$$

$$E^{\star} = \frac{1}{\frac{1-\nu_1^2}{E_1}+\frac{1-\nu_2^2}{E_2}} \quad (6)$$

$$p_{max} = \frac{1}{\pi}\left(\frac{6FE^{\star 2}}{R^2}\right)^{1/3} \quad (7)$$

2.4 Friction testing

The lubricants were tested on a $forceboard^{TM}$ friction tester which can be seen in figure 18. The friction tester acts as a sliding test where the rod is fastened by screws in the holder. In Our setup we have chosen to drag the pin while recording the coefficient of friction. The software used to record parameters such as vertical force, horizontal force, COF, time, displacement and sliding speed was the $forceboard^{TM}$ analyzer which is included with the forceboard.

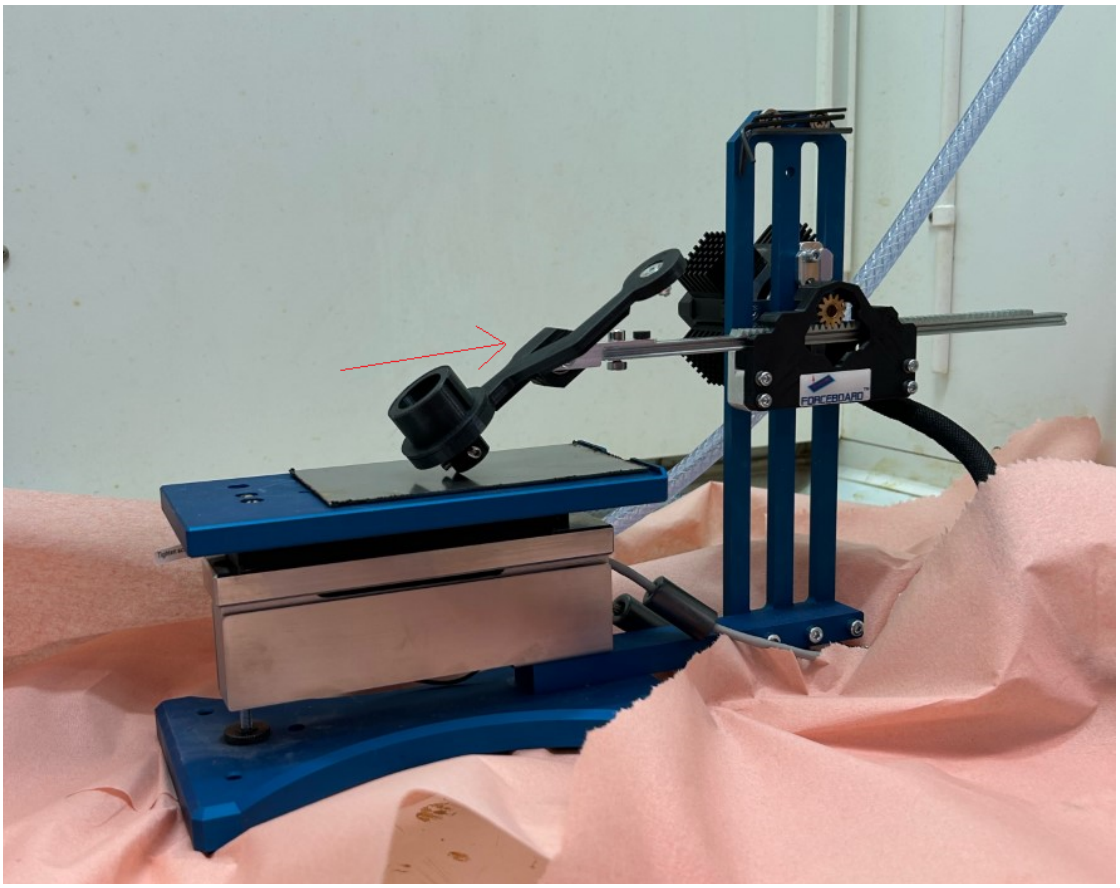

Figure 18. Force board setup.

A slight tilt when setting up the pin placement was set so that several runs of each pin could be recorded. This makes the normal load be somewhat different than the added load itself since the force will be divided into vertical and horizontal force vectors. The tilt angle remained consistent throughout all the tests. The angle was never taken into consideration while recording which is why the added load, normal to the plane is stated in the result section. In reality the true normal load is slightly less, but the difference is minimal. The friction coefficient is still valid as it is calculated by the force vectors during recording.

Solid lubricant powders made from tiny particles which can cause harm to the lungs are used while testing which is why a safety protocol had to be made and followed during experimentation. It was determined that gloves and respirator masks had to be used throughout the whole testing period. The pouches with the content could only be opened and handled under a fume hood.

2.4.1 Procedure

A procedure to carry out the experiment was established to make sure every test had the same foundation to yield a fair and correct reading. This was important as over 50 runs were conducted.

The settings of the rigg while conducting the tests were constant and set to be the following:

- Motor speed (sliding speed): 5 mm/s
- Motor travel (sliding distance): 20 mm

The procedure contained the steps bellow:

1. Clean the plate and pin with ethanol. Visible inspection to make sure no visible dirt or scratches appear on the surface that can render the data incorrect.
2. Place the rectangular plate with the short side against the supporting frame.
3. Fasten the pin in the holder, place it onto the surface of the plate and zero the vertical and horizontal forces in the analytic software (this is done to establish a baseline of the normal force).
4. Add the desired load and zero the horizontal force in the software. The horizontal force yields a friction coefficient even though in theory it should be 0 since the pin is not moving. This is most likely due to the pin being slightly tilted which divides the added load in force vectors.
5. Record the run.
6. Loosen the pin, rotate it a few degrees and follow steps 3-5 again.

The solid lubricant is added between steps 2-3. A teaspoon of the powder is evenly dispersed on the plate and then buffed to make sure every part of the surface is covered, excess powder is dispatched. The same is done for the contact point of the pin. When testing the lubricants in wet conditions two-three teaspoons of water, ethanol or oil is added to the surface of the plate and a teaspoon of the powder is then added and mixed into a slurry. The slurry is lightly buffed onto the surface.

3.0 Results

3.1 Designing the experiment

Stainless Steel 304 will be used as a reference material where solid lubricants will be added. The solid lubricants will be tested under dry conditions as well as wet conditions. Parameters such as radius of the spherical indenter and load are decided by figure 19 and 20, which can be seen below.

3.1.1 Radius of pin

The spherical indenter is determined to have a radius of 10 mm or larger to minimize the amount of plastic deformation upon the surface of the reference material. The body of the rod itself can have a maximum radius of 6 mm radius. Therefore the rod needs to have an end piece with the determined radius (>10 mm). In figure 19, it can be seen that with an increasing radius up to 10 mm and larger with a set load of 4.91 N, the maximum shear stress declines towards acceptable values.

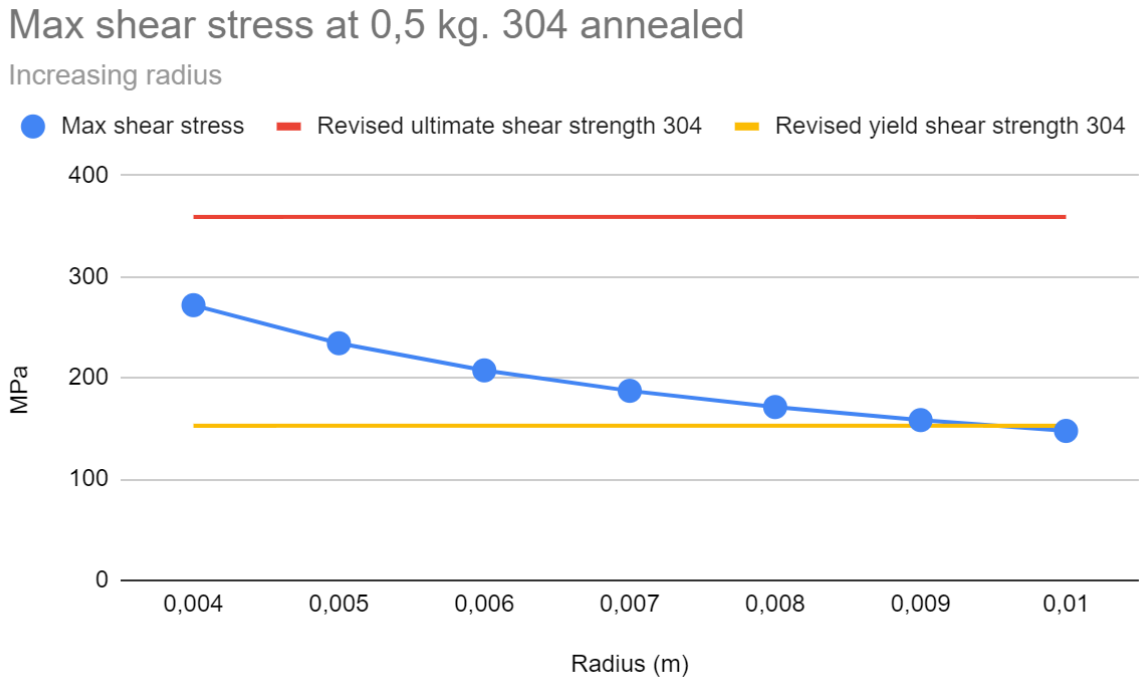

Figure 19. Max shear stress at 0,5kg load vs. pin radius.

3.1.2 Load

Looking at figure 20 below for reference, the maximum shear stress declines with decreasing load. Since the ideal test for this application would be to have no plastic deformation, the load during testing is determined to be 4,91 N (0,5 kg) and 14,73N (1,5 kg) to examine what the results of exceeding the theoretical yields shear strength would be.

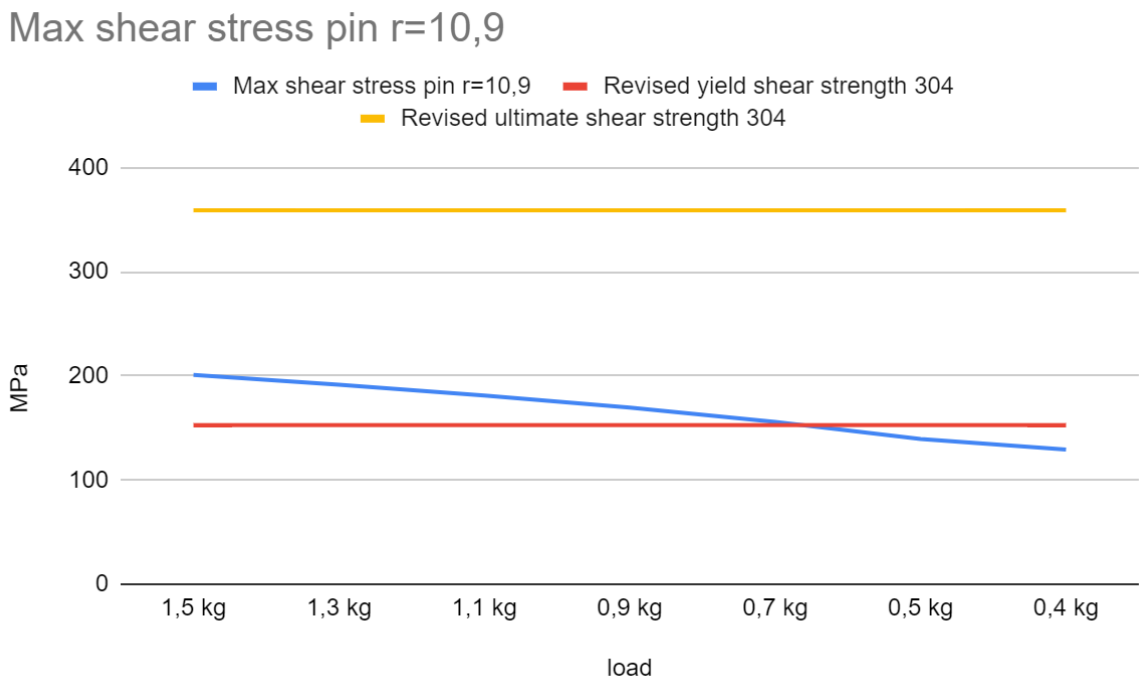

Figure 20. Max shear stress with a pin radius of 10,9 mm vs. load.

3.2 Self-mated Stainless steel 304

A base coefficient of friction is experimentally obtained, this will act as a reference to determine whether the addition of the solid lubricant in powder form decreases or increases the COF.

Looking at figure 21, it can be seen that the friction during the first few seconds is 0, this is due to the sliding motion has not been initiated yet. Furthermore the first bump of the friction curve will be disregarded since the COF will be higher due to static friction. After the cantilever has dragged for 20 mm it stops fully but the program still records a COF even though it should be 0. In the charts, where the cantilever stops dragging can be characterized by the COF stabilizing dramatically and the mean value typically decreases. This is true to all charts obtained.

For all of the tests, to collect a fair and justified COF, the mean value will be taken from the area of the graphs where the green rectangle is placed as seen in figure 21 a). The values can be seen in table 4, both the separate average COF's of each chart in figure 21 and 22, are displayed and then compiled to a mean COF. The reference coefficient of friction was measured to be 0,221at a load of 4,91N and 0,249 at a load of 14,73N.

Results in table 4 portraits that the coefficient of friction is increased at high loads. This is most likely to be a consequence of plastic deformation and more adhesion due to heavier load. It also yields a more stable and less sporadic chart in terms of coefficient of friction.

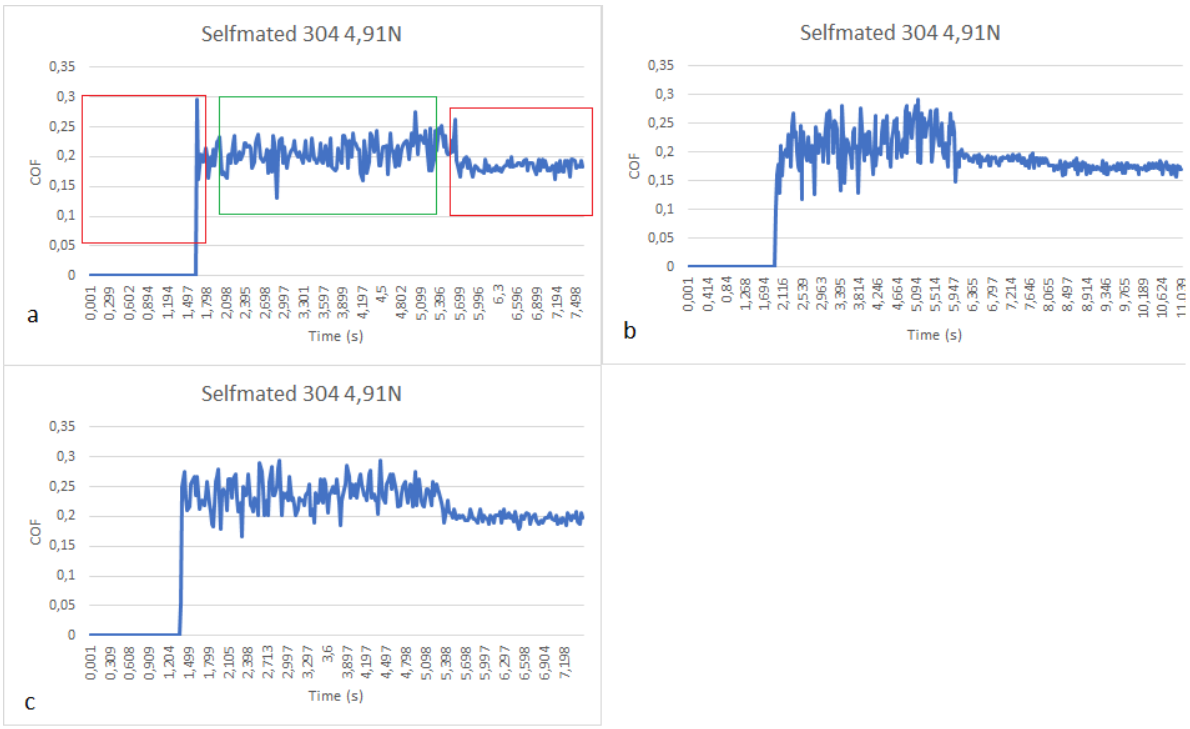

Figure 21. Coefficient of friction graphs of self-mated stainless steel 304 recorded during testing with a load of 4,91N.

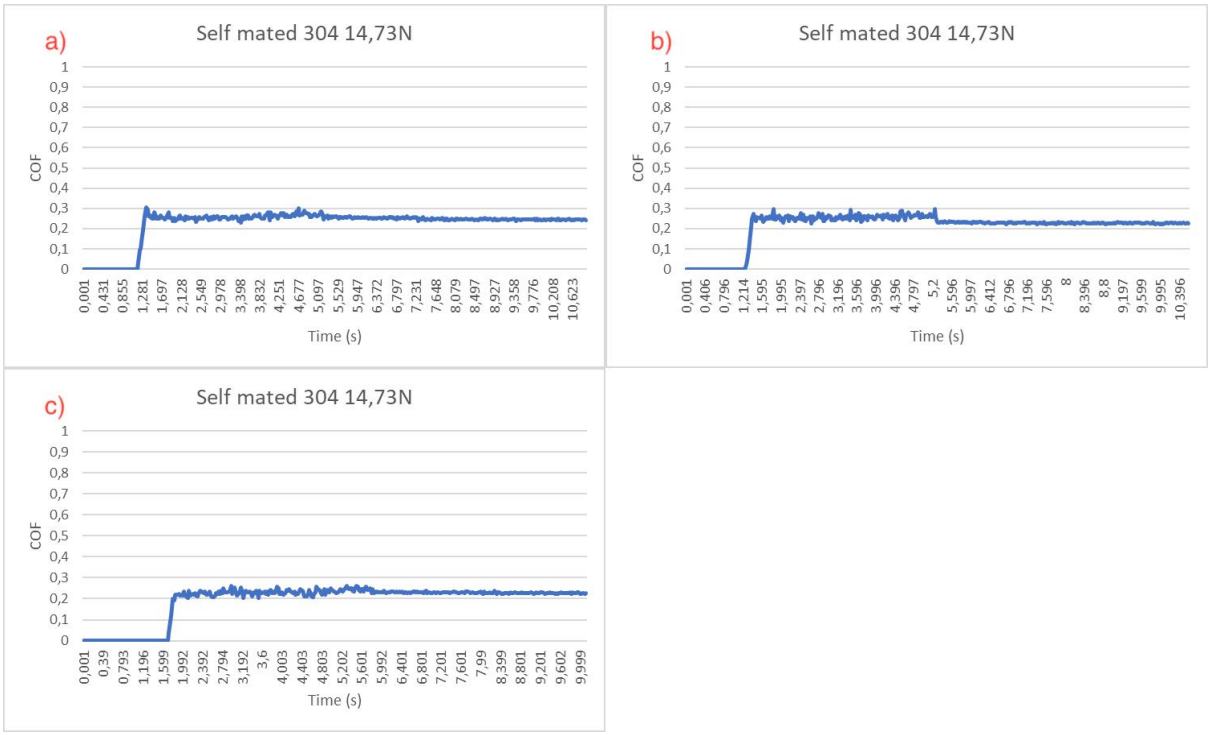

Figure 22. a, b and c. Coefficient of friction graph of self-mated stainless steel 304 recorded during testing with a load of 14,73N

Table 4. Separate average COF and compiled average COF of stainless steel 304 self-mated with a load of 4,91N and 14,73N.

	Average COF (4,91N)	AvarageCOF (4,91N)	Average COF (14,73N)	AvarageCOF (14,73N)
a	0,208	0,221	0,260	0,249
b	0,219		0,256	
c	0,237		0,231	

3.3 Addition of hexagonal boron nitride powder

3.3.1 Dry conditions

The addition of h-BN powder seems to increase the friction. The mean values in table 5. shows a higher coefficient of friction than the reference material which was unexpected. This can be an effect of not applying the powder in an appropriate way or other factors such as agglomeration which could be observed during testing. The agglomeration was seen on the face of the pin. Before each test the agglomerated powder was brushed off. This h-BN powder had the largest particles of the solid lubricants that were tested, the particle size was 10 micrometers which could have been a crucial factor. As for the volatility of the curve in Figure 23, no obvious factors other than the influence of shape and size of the particles could be found. The curve stabilizes a bit and does not spike as much when a higher load is applied seen in Figure 24.

The addition of h-BN yielded an increase of COF by 144,8% respectively 135,4% when comparing it to the established baseline which can be seen in table 5.

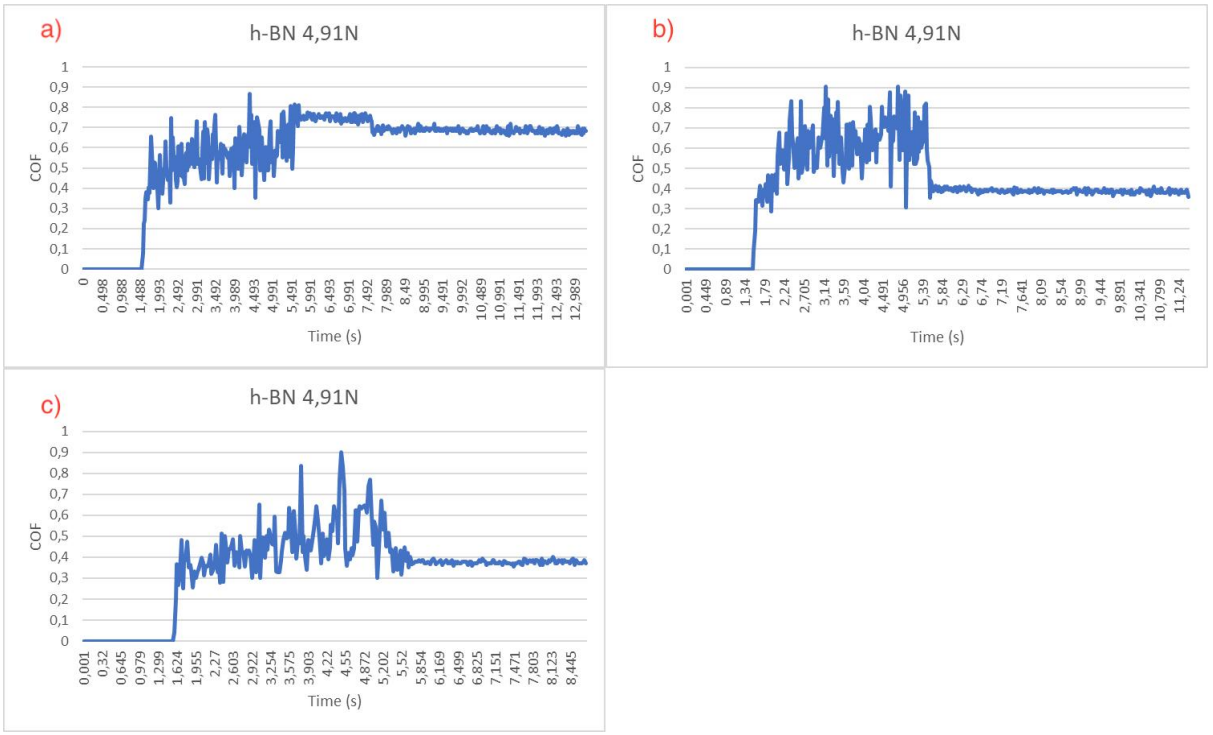

Figure 23. Coefficient of friction graph with the addition of h-BN powder under a load of 4,91N.

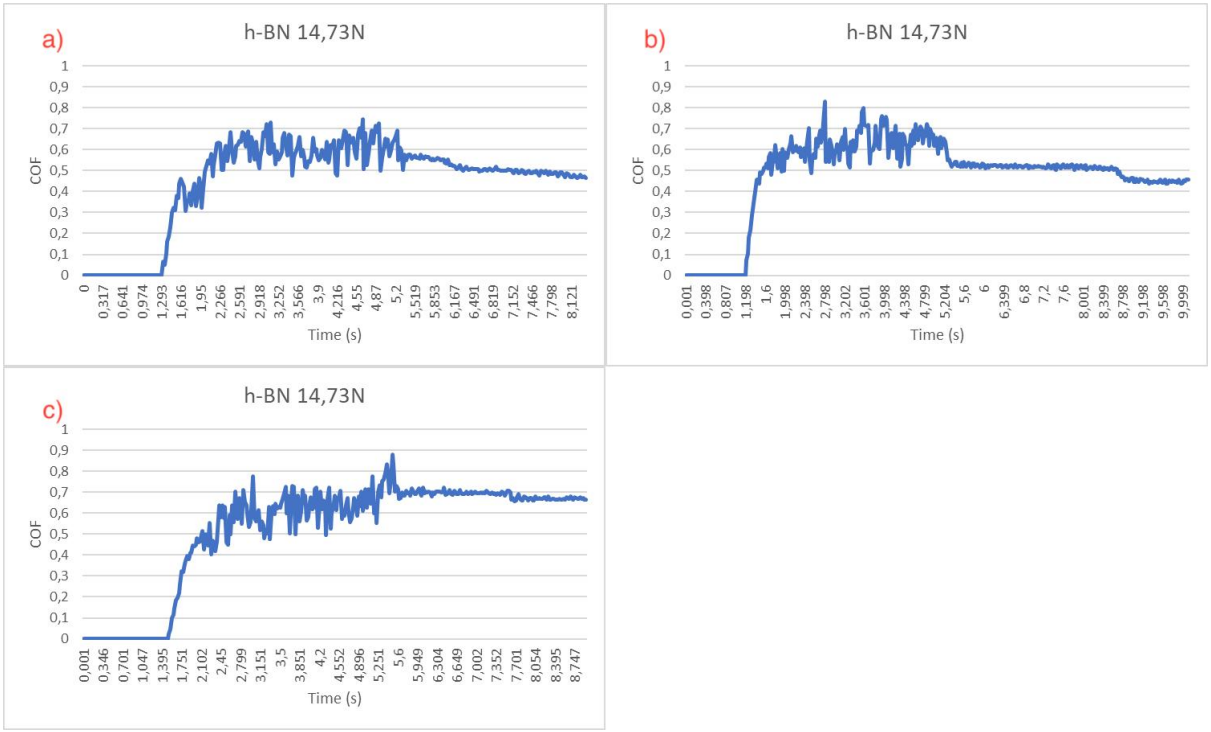

Figure 24. Coefficient of friction graph with the addition of h-BN powder under a load of 14,91N

Table 5. Separate average COF and compiled average COF of stainless steel 304 self-mated with the addition of h-BN powder under a load of 4,91N and 14,73N.

	Average COF (4,91N)	AvarageCOF (4,91N)	Average COF (14,73N)	Avarage COF (14,73N)
a	0,561	0,541	0,570	0,586
b	0,602		0,607	
c	0,461		0,582	

3.3.2 Wet conditions

Testing h-BN in wet conditions seemed to increase the effectiveness of the lubrication properties leading to decreasing the COF in respect to dry conditions as seen in figure 25. However the overall effectiveness of the addition is still worse than self-mating stainless steel 304. h-BN in wet conditions gave a COF of 0,362 when suspended in an ethanol slurry and 0,459 in a water slurry which can be seen in table 6. This is an increase of 45,4% respectively 84,3% to the COF compared to the reference.

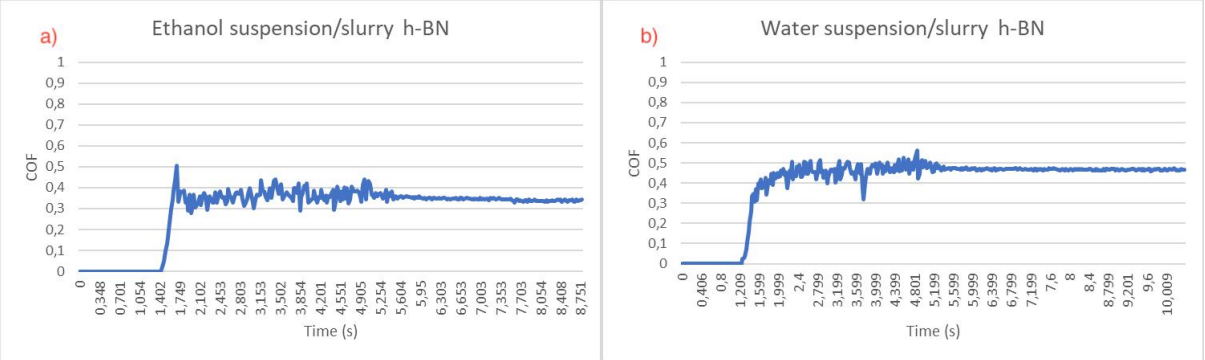

Figure 25. Coefficient of friction graph with the addition of h-BN powder under 14,73N in wet conditions. a) h-BN powder mixed into a slurry with ethanol. b) h-BN powder mixed with water into a slurry.

Table 6. Average coefficient of friction of the graphs in figure 25.

	AvarageCOF (14,73N)
a	0,362
b	0,459

3.4 Addition of Tungsten disulfide powder (WS_2)

3.4.1 Dry conditions

It can be derived from figure 26 and 27, that the added WS_2powder decreases the friction between the plate and pin both at low loads and higher loads. In table 7 the mean COF during the sliding test was measured to 0,162 under 4,91N load, at the load of 14,73N, it was even less and measured to 0,147. When comparing the coefficient of friction in this experiment to the reference it can be seen that with increased normal load, the COF decreases when WS_2 powder has been added.

Comparatively, the addition of WS_2powder reduced the COF by 26,7% respectively 41% to the reference.

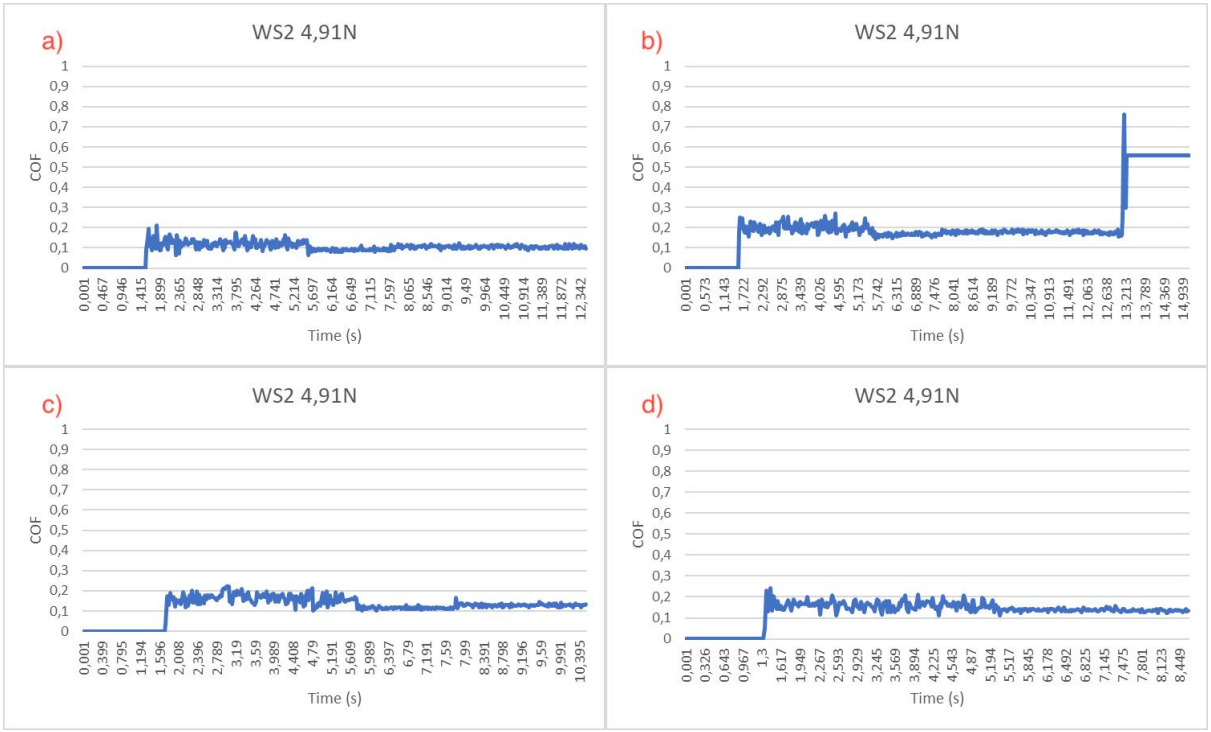

Figure 26. Coefficient of friction graphs with the addition of WS_2 powder under a load of 4,91N

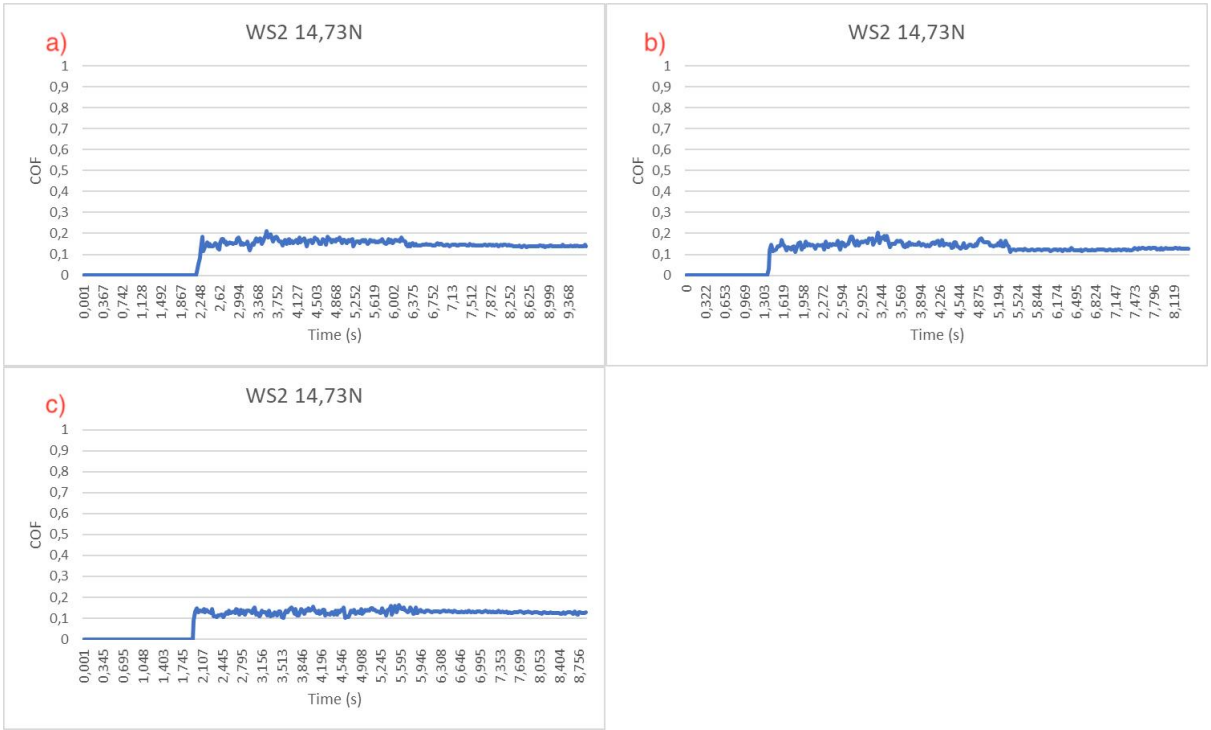

Figure 27. Coefficient of friction graphs with the addition of WS_2 powder under a load of 14,73N

Table 7. Separate average COF and mean COF of stainless steel 304 self-mated with the addition of WS_2 powder under a load of 4,91N and 14,73N.

	Average COF (4,91N)	AvarageCOF (4,91N)	Average COF (14,73N)	Avarage COF (14,73N)
a	0,123	0,162	0,161	0,147
b	0,202		0,149	
c	0,163		0,131	
d	0,161		-	

3.4.2 Wet conditions

Conducting the experiment in wet conditions with WS_2 powder shows that it inhibits its lubricating properties in respect to the experimentally obtained data in dry conditions. Compared to the reference of steel on steel with no lubrication, an ethanol slurry decreased the COF by a tiny bit, which virtually seems insignificant (4% decrease). A mixture of water and WS_2 powder increased the COF by 33,7%. COF graphs can be seen in figure 28 and the corresponding numbers in table 8.

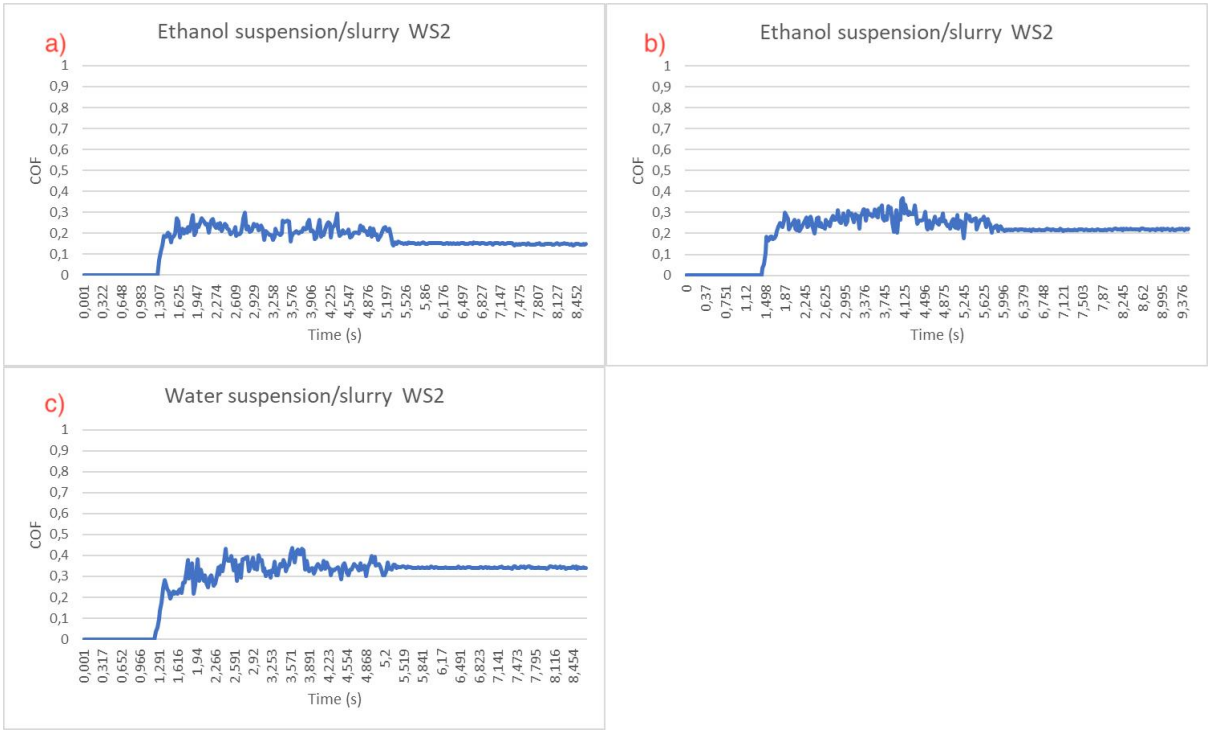

Figure 28. Coefficient of friction graphs with the addition of WS_2 powder under a load of 14,73N in wet conditions. a, b) WS_2 powder mixed with ethanol into a slurry. c) WS_2 powder mixed with water into a slurry.

Table 8. Mean COF of stainless steel 304 self-mated with the addition of WS_2 powder under a load of 14,73N in wet conditions.

	Average COF (14,73N)
a, b	0,239
c	0,333

3.5 Addition of molybdenum disulfide (MoS_2)

3.5.1 Dry conditions

MoS_2 in dry conditions proved to be the compound that decreased the friction the most out of the three tested. In Figure 29 and 30, some aggressive spikes in the charts can be seen, this has been determined to be defects such as scratches on the plate surface. At the load of

4,91N the graphs look pretty volatile but as figure 30 shows, at heavier loads the COF stabilizes quite a lot, keeping in mind that the vertical axis scale influences the volatility of the line.

Mean values of the COF from the graphs have been compiled in Table 9 and states that the average COF during the sliding tests for 4,91N is 0,098. Mean COF value for tests conducted with 14,73N is 0,085. The addition of MoS_2 powder therefore reduced the COF by 55,7% respectively 65.7%.

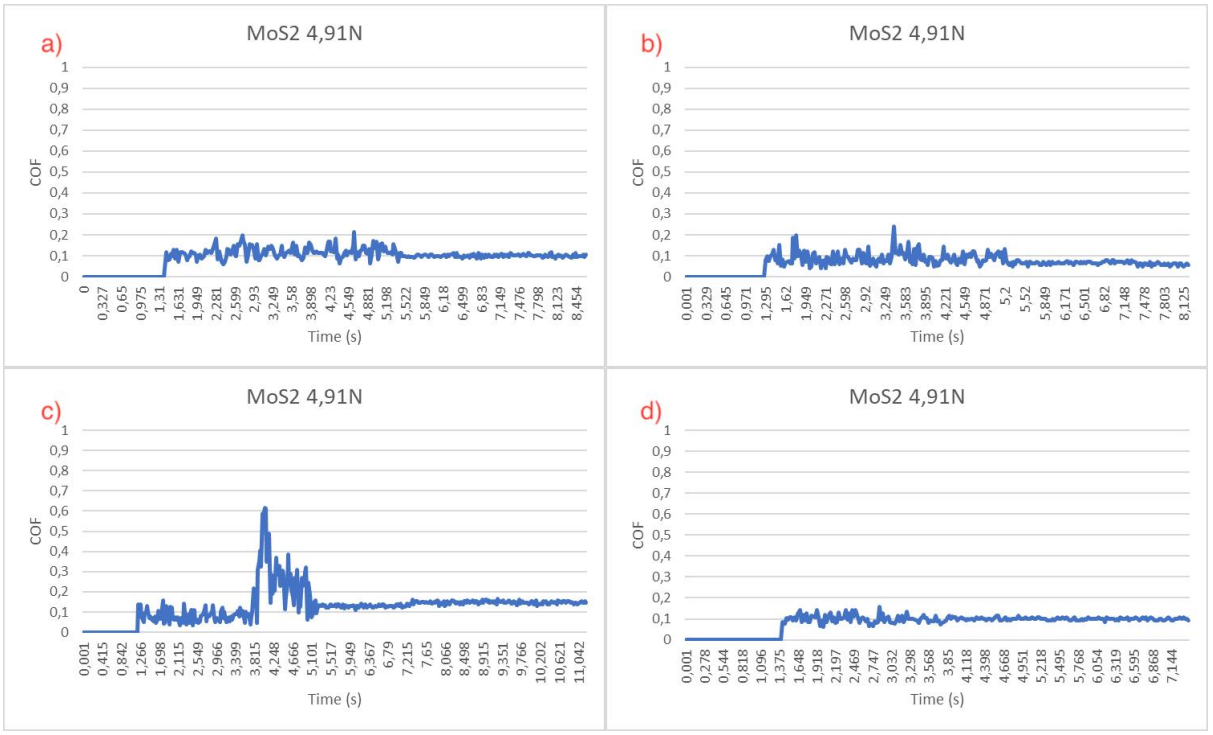

Figure 29. Coefficient of friction graphs with the addition of MoS_2 powder under a load of 4,91N in dry conditions.

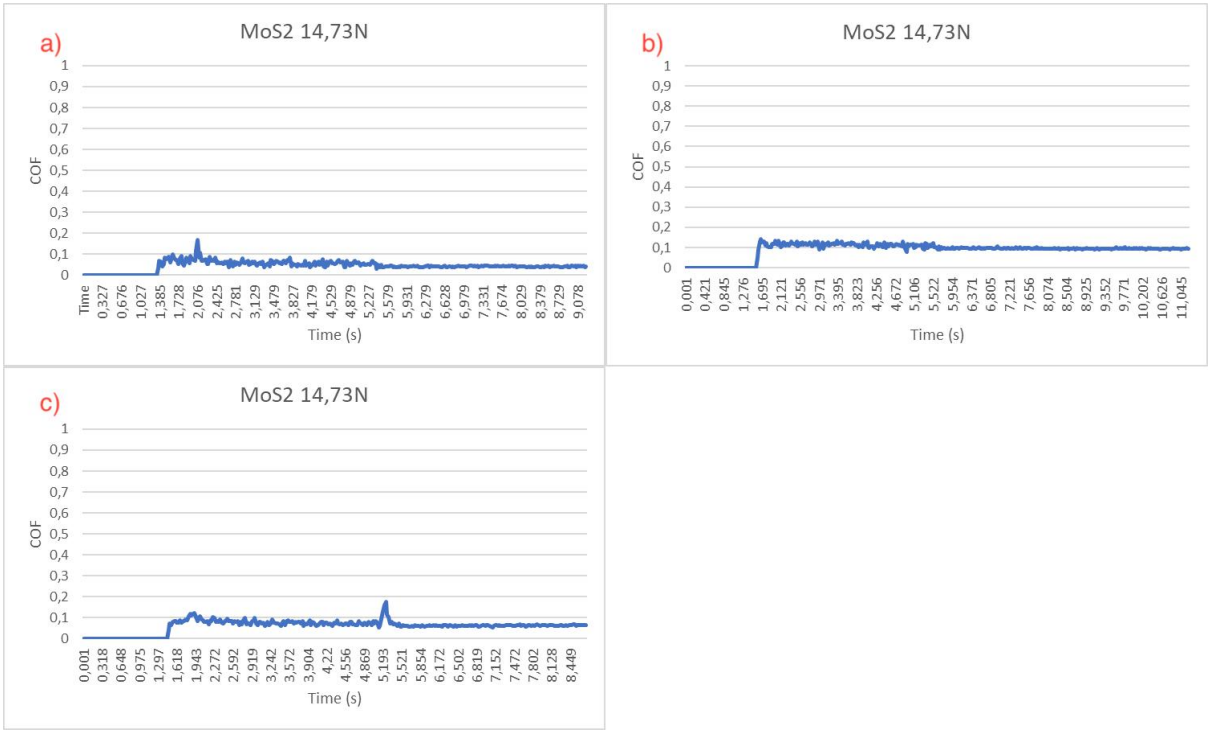

Figure 30. Coefficient of friction graphs with the addition of MoS_2 powder under a load of 14,731N

Table 9. Separate average COF and mean COF of stainless steel 304 self-mated with the addition of MoS_2 powder under a load of 4,91N and 14,73N in dry conditions.

	Average COF (4,91N)	Average COF (4,91N)	Average COF (14,73N)	Average COF (14,73N)
a	0,118	0,098	0,061	0,085
b	0,091		0,114	
c	0,083		0,080	
d	0,101		-	

3.5.2 Wet conditions

In slurry form the mixture lost some of its lubricating effects compared to the dry tests. It can however be concluded when looking at Table 10 that an ethanol slurry of MoS_2 powder reduces the COF by 40,2%, a water slurry increased the COF by 60,6% and an oil based slurry decreased the COF by 29,3%. Corresponding COF graphs can be seen in figure 31.

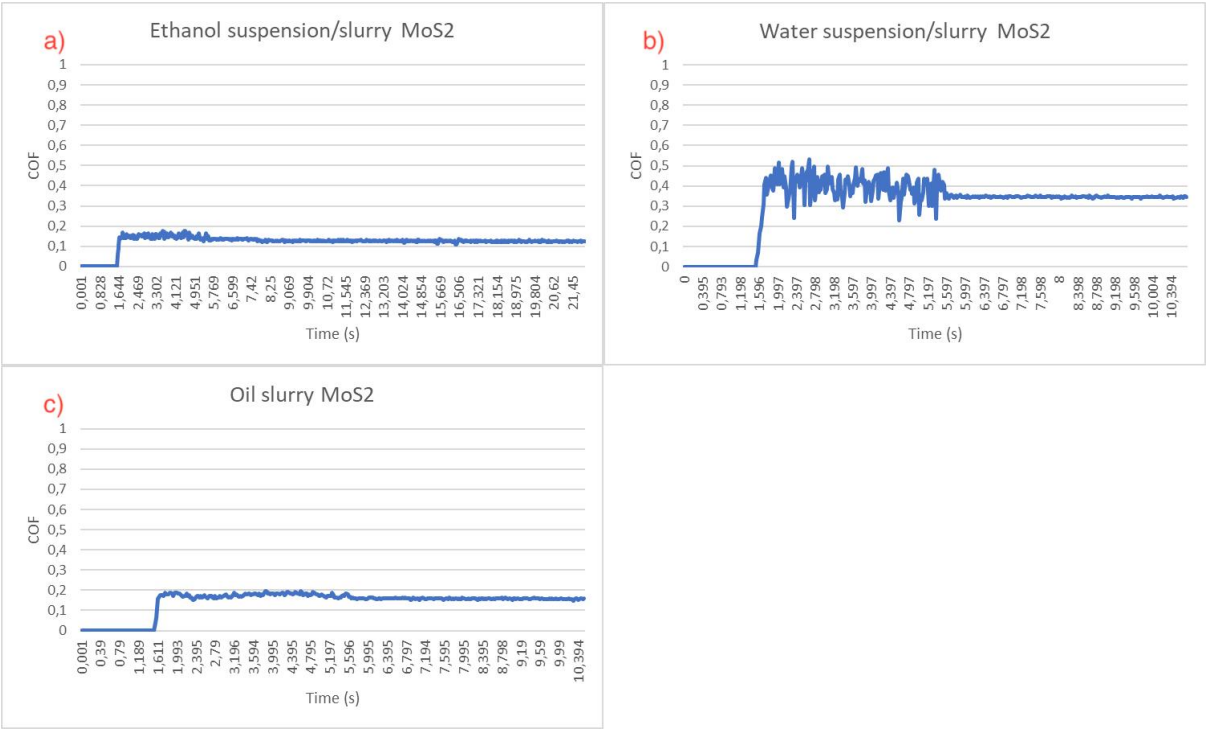

Figure 31. Coefficient of friction graphs with the addition of MoS_2 powder under a load of 14,73N in wet conditions. a) MoS_2powder mixed with ethanol into a slurry, b) MoS_2 powder mixed with water into a slurry, c) MoS_2 powder mixed with oil into a slurry

Table 10. Mean COF of stainless steel 304 self-mated with the addition of MoS_2 powder under a load of 14,73N in wet conditions.

	Average COF (14,73N)
a	0,149
b	0,400
c	0,176

3.6 Compiled results

To make the results more easily read and comparable, all averages when tested at 14,73N load, have been compiled in table 11 below.

Table 11. COF results with a load of 14,73N and 4,91 for dry conditions,

Condition/COF	Self-mated (no added powder)	Self-mated (added h-BN powder)	Self-mated (added WS_2 powder)	Self-mated (added MoS_2 powder)
Dry 4,91N: 14,73N:	0,221 (ref) 0,249 (ref)	0,541 (+144,8%) 0,586 (+135,3%)	0,162 (-26,7%) 0,147 (-41%)	0,098 (-55,7%) 0,085 (-65,9%)
Wet (ethanol) 14,73N	-	0,362 (+45,4%)	0,239 (-4%)	0,149 (-40,2%)
Wet (water) 14.73N	-	0,459 (+84,3%)	0,333 (+33,7%)	0,400 (+60,6%)
Wet (oil) 14,73N	0,229	-	-	0,176 (-29,3% resp. -23,1%)

4. Discussion

In this section the results and possible sources of error will be discussed. Due to limitations and lack of testing equipment, experiments conducted could not be designed in a way to imitate conditions in the RANTOR engine. Therefore the experiments only included testing at room temperatures in dry and wet conditions even though the environment in the engine is high temperature and high pressure with supercritical steam as a medium. Comparing my tests to the wear map in section 1.5, we are using low loads at low sliding speed which puts us in the slight wear area. Therefore no severe mechanical damage could be observed upon any surface.

4.1 Friction tests

During testing, some sources of errors were found, these are stated and discussed below.

Inconsistency of surface roughness

In this thesis, surface roughness was never measured which is a fault since it can influence the COF significantly. This was however compensated by repeating the friction tests three times on different areas of the surface, the average value of these was computed from recorded measurements. Additionally, surface roughness of the plates tested does not differ too much across the total area, thus the somewhat inconsistent COF measured at times most likely has to do with other mechanisms, such as agglomeration of particles.

Amount of powder added

The amount of powder material added to the surface was never measured, it was however buffed in and excess was wiped from the testing surface in dry conditions. As for wet conditions a simple slurry/suspension was mixed on the surface resulting in inconsistency of wt.% added to the medium.

COF recorded after a run

Seen in the result section, a dynamic COF was recorded consistently after the 20 mm movement was finished, which is not theoretically possible since the pin is in a fixed position not moving. This was probably due to the pins being longer than necessary which could give rise to a spring effect once it has come to a halt, resulting in a horizontal force vector pushing on the plate and therefore recording a COF. This source of error is also increased because of the slight tilt the pins were mounted with.

4.1.2 Steel-steel

Self-mated steel during testing yielded a low COF which was rather unexpected, since some sources state that the dynamic COF of stainless steel 304 is almost twice as large as what was measured. The low COF of self-mated 304 gathered is most likely an effect of using low sliding velocity as well as low loads during testing. This topic has been covered and is supported by several reports such as a study made by Nuruzzaman & Chowdhury [28] 2012. The authors [28], conducted several experiments where both normal load and sliding speed was varied and both of the parameters pointed to a decrease of dynamic COF when using slow velocities and low normal loads.

However the initially low dynamic COF should not be an issue since all parameters such as loads and sliding speed were kept constant. Furthermore the measured COF of stainless steel 304 is similar to the one tested and measured by Chowdhury et al [29].

As for the wear a visual inspection was made on the surfaces of both the plate and pin, at the lower load of 4,91N no visible scratches could be seen on either surface which indicates that during this contact pressure the maximum shear stress during sliding was below the elastic shear strength, which was calculated in section 3.1.2. On visual examination of runs where a heavier load (14,73N) was applied, marks on both surfaces could be seen which indicated that the shear stress induced plastic deformation upon the surfaces which is also in line with what was calculated in section 3.1.2.

4.1.3 h-BN

Unexpectedly the addition of h-BN in dry conditions yielded more than 100% increase of COF. The particles in this powder had an average diameter of 10 microns which was the largest of the three powders tested. It is known that larger particles in specific shapes give rise to abrasion and ploughing, which means it is possible that when introducing the h-BN particles this had an opposite effect of what was intended. However no visible abrasion or ploughing marks caused by particles could be observed with a visual inspection.

Further the particles could be seen agglomerating on the base of the pin while sliding, this is the most probable cause of the increase of COF. Even though the powder was buffed into the surface and excessive powder was brushed off, particles would still agglomerate at previously stated area.

Mixing h-BN in ethanol and water seemed to increase the efficiency of lubricating properties, yielding a lower COF than in dry conditions but still worse than self-mating 304 steel. The main cause for this could be that the particles are better dispersed when mixed into a slurry and then buffed onto the surface so that the small particles more easily can fill surface cavitations and create a protective-lubricant film. A study [17] referenced in the literature review, suggests that the efficiency of the h-BN dispersion is heavily dependent on small concentrations of the additive to yield reduction of COF along with being very well dispersed which can be achieved by using an ultrasonic dispersion device.

In our experiments the concentration was not taken into consideration as well as dispersing it in the liquids too well. A teaspoon of the powder was mixed with 2-3 teaspoons of water, mixing it into a slurry and then lightly smeared on the surface and then tested in the friction tester. A reduction of COF relative to the reference test could probably have been achieved if correct concentration of h-BN was used. The main reason why higher concentrations of h-BN does not work too well is that the particles tend to agglomerate thus inhibiting the mixture's ability to supply the contact area with a constant feed of particles.

4.1.4 Tungsten disulfide

Results showed that by buffing tungsten disulfide powder under dry conditions onto the stainless steel surface, the friction coefficient can be reduced heavily. This is due to the particles creating a thin lubricant film with good adherence and low shear-strength yielding a lower COF. Some agglomeration formed on the pin surface but once it was wiped away no further build ups of material could be seen. The small agglomeration which was observed was most likely excess particles that had not been wiped away properly. The reduced COF kept through several testing runs in combination with no further agglomeration supports the statement that a thin lubricating film with good adherence had formed on both of the surfaces.

Once mixed with ethanol a very small reduction of friction in comparison with the reference material could be measured. This could be that the slurry and dispersion of particles inhibits the lubricant's ability to adhere to the surface properly, also agglomerations were observed meaning that the particles did not interact well with the surface.

Mixed in water the COF increased quite heavily. Particles did not mix well and floated up to the water surface thus being suspended by the surface tension of the water. The increase of COF is thought to be due to particles not adhering to the steel surface, agglomeration on the

water surface causing the pin to have to be dragged through added resistance thus resulting in an increase of COF.

In the literature study [19] [20] it was found that tungsten disulfide as an additive in oil is very promising, reducing COF and increased wear resistance, if it is added in small specific concentrations.

4.1.5 Molybdenum disulfide

Molybdenum disulfide Proved during testing to be the most efficient at reducing the COF dry in conditions out of the three powders tested. In dry conditions the additive fills crevasses and forms a thin lubricating film (just like tungsten disulfide) with good adherence, reducing surface to surface contacts between the two reference materials. Through the literature study it was found that molybdenum disulfide is often used in dry conditions as it wont agglomerate to easily

The additive performed better than the previous two materials when dispersed in ethanol, yielding a lower COF than the reference material but still higher COF than when tested under dry conditions. Mixed with water the particles flow to the water surface and rest on top of the surface tension where it agglomerates, not interacting with the surfaces of the plate and pin, therefore an increase of COF in comparison to the reference can be observed. Theory of why the COF increases when the particles flow to the surface is the same as for tungsten disulfide.

Further the molybdenum disulfide was tested in an oil mixture, reducing the COF compared to the reference, however it performed worse than when being observed under dry conditions. As mentioned earlier molybdenum disulfide particles tend to agglomerate in oil which was also observed during the friction tests. Additionally it could be seen that the agglomerated particles were “pushed” away from the surface in contact when the pin was in movement

Studies [21] [23] referenced in the literature study shows great success for molybdenum disulfide as an additive in oil, also at very low concentrations when being mixed extensively and thoroughly.

4.1.6 Medium

The three additives tested and researched performed seemingly badly when tested in wet conditions, especially when suspended in water. When suspended in an ethanol medium they were more easily dispersed and did not float to the top. This most likely has to do with ethanol having weaker intermolecular forces which is why it has a weaker surface tension.

No research was found on tungsten disulfide or molybdenum disulfide lubricating properties in water suspension, all papers about these two as an additive to improve COF and wear resistance were conducted in different oil mediums. This suggests that in the current day and age there is no benefit of using them as an additive to reduce friction in a water medium. However, as an additive in oil they both show great success.

One study [17] on h-BN as an additive in water based lubrication was referred to in the literature study, the study presented results of h-BN in a water mixture lowered the COF significantly. h-BN was also found to reduce the COF in oil mediums according to a study [16] referred to in the literature review.

4.2 Utilization in the RANOTOR engine

As for utilizing any of these materials as an additive into the steam in the engine, the results in combination with the literature study points to difficulties of agglomeration and effectiveness in a water medium. However since the additives have not been tested in a steam environment it is impossible to simply guess how they would react. Most importantly it is unknown whether the small particles would be able to travel within the steam droplets through the engine and reduce the COF in the desired place, which is between the piston rings and the cylinder block. The chances of agglomeration are high thus clogging the closed system is something that also would have to be further tested.

Testing the powdered materials in dry conditions mimics the effects of using them as a super thin coating. The particles form a thin lubricating-protective layer with good adherence to the surface which is the basics of utilizing a coating. Since all three of the materials tested meet the environmental requirements of the engine, I suggest further testing by coating the desired areas in the engine with the materials which were friction tested in this thesis.

5. Conclusion

- h-BN did not decrease COF in any condition.
- WS_2 decreased COF by 41% in dry conditions acting as a thin protective-lubricating film. Suspended in water COF increased and no significant change when it was suspended in ethanol.
- MoS_2decreased COF by 65,7% in dry conditions acting as a thin protective-lubricating film. Suspended in water COF increased significantly, ethanol suspension decreased COF by 40,2% and an oil based slurry decreased the COF by 29,3%.
- The lubricating mechanism is interlayer slippage derived from the solid lubricants easily sheared layers, when they are applied correctly to the steel surface, thus creating a thin protective-lubricating film.
- Additives in the steam are likely to clog the system due to the particles' attraction to agglomerate ***if they were able to travel through the engine suspended in steam droplets.***
- Further testing and research should be focused on the use of h-BN, $WS_2$and MoS_2 coatings as it exhibits promising potential.

References

[1]: Sources of Greenhouse Gas Emissions [Internet]. Environmental Protection Agency; [cited 2023 Jun 4]. Available from: https://www.epa.gov/ghgemissions/sources-greenhouse-gas-emissions

[2]: Jouhara H, Olabi AG. Editorial: Industrial waste heat recovery. Energy. 2018;160:1–2.

[3]: Tung SC, McMillan ML. Automotive tribology overview of current advances and challenges for the future. Tribology International. 2004;37(7):517–36.

[4]: Fallqvist M. Tribology: Friction MTAD19 2022

[5]: Fallqvist M. Tribology: Sliding wear MTAD19 2022

[6]: Fallqvist M. Tribology: Wear by hard particles MTAD19 2022

[7]: Fallqvist M. Tribology: Lubrication MTAD19 2022.

[8]: Technology [Internet]. [cited 2023 Mar 10]. Available from: https://www.ranotor.se/projects-3

[9]: Samuelsson J. Material analysis for a rotating inlet valve: Sliding contact in an oil-free super-critical steam environment [Internet]. 2022 [cited 2023 May 24]. Available from: https://kau.diva-portal.org/smash/record.jsf?dswid=-7499&pid=diva2%3A1699750&c=4&searchType=SIMPLE&language=sv&query=ranotor&af=%5B%5D&aq=%5B%5B%5D%5D&aq2=%5B%5B%5D%5D&aqe=%5B%5D&noOfRows=50&sortOrder=author_sort_asc&sortOrder2=title_sort_asc&onlyFullText=false&sf=all

[10]: Boron nitride [Internet]. Wikimedia Foundation; 2023 [cited 2023 Mar 12]. Available from: https://en.wikipedia.org/wiki/Boron_nitride

[11]: Roy S, Zhang X, Puthirath AB, Meiyazhagan A, Bhattacharyya S, Rahman MM, et al. Structure, properties and applications of two‐dimensional hexagonal boron nitride. Advanced Materials. 2021;33(44):2101589.

[12]: Falin A, Cai Q, Santos EJG, Scullion D, Qian D, Zhang R, et al. Mechanical properties of atomically thin boron nitride and the role of Interlayer Interactions. Nature Communications. 2017;8(1).

[13]: Park J-H, Sudarshan TS. Chemical vapor deposition. Materials Park, OH: ASM International; 2001.

[14]: Shi Y, Hamsen C, Jia X, Kim KK, Reina A, Hofmann M, et al. Synthesis of few-layer hexagonal boron nitride thin film by chemical vapor deposition. Nano Letters. 2010;10(10):4134–9.

[15]: Çamurlu HE. Effect of NA2CO3 on hexagonal boron nitride prepared from urea and boric acid. Ceramics International. 2011;37(6):1993–9.

[16]: Ma Z-S, Ding H-L, Liu Z, Cheng Z-L. Preparation and tribological properties of hydrothermally exfoliated ultrathin hexagonal boron nitride nanosheets (bnnss) in mixed NaOH/Koh Solution. Journal of Alloys and Compounds. 2019;784:807–15.

[17]: Bin Abdollah MF, Amiruddin H, Alif Azmi M, Mat Tahir NA. Lubrication mechanisms of hexagonal boron nitride nano-additives water-based lubricant for steel–steel contact. Proceedings of the Institution of Mechanical Engineers, Part J: Journal of Engineering Tribology. 2020;235(5):1038–46.

[18]: Ding J, Feng A, Li X, Ding S, Liu L, Ren W. Properties, preparation, and application of tungsten disulfide: A Review. Journal of Physics D: Applied Physics. 2021;54(17):173002.

[19]: Wu N, Hu N, Zhou G, Wu J. Tribological properties of lubricating oil with micro/nano-scale WS2 particles. Journal of Experimental Nanoscience. 2017;13(1):27–38.

[20]: Shi C, Mao D, Feng H. Preparation of tungsten disulfide motor oil and its tribological characteristics. Journal of Central South University of Technology. 2007;14(5):673–8.

[21]: Gupta D, Chauhan V, Kumar R. A comprehensive review on synthesis and applications of molybdenum disulfide (MOS2) material: Past and recent developments. Inorganic Chemistry Communications. 2020;121:108200.

[22]: He Z, Que W. Molybdenum disulfide nanomaterials: Structures, properties, synthesis and recent progress on hydrogen evolution reaction. Applied Materials Today. 2016;3:23–56.

[23]: Farsadi M, Bagheri S, Ismail NA. Nanocomposite of functionalized graphene and molybdenum disulfide as friction modifier additive for lubricant. Journal of Molecular Liquids. 2017;244:304–8.

[24]:Zhu X. Tutorial on Hertz Contact Stress - University of Arizona [Internet]. 2012 [cited 2023 Jun 7]. Available from:

https://wp.optics.arizona.edu/optomech/wp-content/uploads/sites/53/2016/10/OPTI-521-Tutorial-on-Hertz-contact-stress-Xiaoyin-Zhu.pdf

[25]: Genov G [Internet]. 2020 [cited 2023 Jan 3]. Available from: https://www.researchgate.net/publication/355208819_REVISITING_THE_RULE-OF-THUMB_DEPENDENCIES_OF_THE_SHEAR_STRENGTH_AND_THE_HARDNESS_ON_THE_YIELD_AND_THE_ULTIMATE_STRENGTHS

[26]: Iron alloy [Internet]. 2020 [cited 2023 Jan 3]. Available from: https://www.makeitfrom.com/material-properties/Annealed-304-Stainless-Steel

[27] Hertzian contact stress calculator [Internet]. [cited 2023 Jan 3]. Available from: https://amesweb.info/HertzianContact/HertzianContact.aspx

[28]: Muhammad Nuruzzaman D, Asaduzzaman Chowdhury M. Effect of load and sliding velocity on friction coefficient of aluminum sliding against different pin materials. American Journal of Materials Science. 2012 Feb 1;2(1):26–31.

[29]: Chowdhury MA, Nuruzzaman DM, Chowdhury MA, Roy BK. Experimental study of friction coefficient and wear rate of turned and ground mild steel surfaces sliding against smooth and rough SS304 counterfaces. Australian Journal of Mechanical Engineering. 2014 Sept 23;12(3):291–304.